Quantum State and Process Tomography of Energy Transfer Systems via Ultrafast Spectroscopy

Supporting Information

Joel Yuen-Zhou, Jacob J. Krich, Masoud Mohseni and Alán Aspuru-Guzik

Contents

I. Properties of $\chi(T)$. Derivation of Equations 1-4 in the article

II. Transition dipoles of the coupled dimer model

III. State preparation. Derivation of Equation 9 in the article

- **A.** Well-separated pulses 1 and 2
- **B.** Overlapping pulses 1 and 2

IV. State detection. Derivation of Equations 14-16 in the article

- **A.** Well-separated pulses 3 and 4
- **B.** Overlapping pulses 3 and 4

V. Overall multiplicative constant

VI. Isotropic averages

VII. Errors in state preparation and detection

VIII. Discussion of the factorizable condition at $T = 0$

IX. Trading frequency control for time delay

X. Secular Redfield model for Markovian dissipation

XI. Reconstruction of $\chi(T)$

A. Reconstruction of the values $\langle P^{p,q,r,s}_{z,z,z,z}(\tau,T,t)\rangle_{iso}$ from the signals $\langle [S_{PE}]^{\omega_1,\omega_2,\omega_3,\omega_4}_{z,z,z,z}(\tau,T,t)\rangle_{iso}$

B. Reconstruction of $\chi(T)$ from $\langle P^{p,q,r,s}_{z,z,z,z}(\tau,T,t)\rangle_{iso}$

C. Choosing sixteen measurements out of the thirty-two heterodyne detections

XII. Scalability

I. PROPERTIES OF $\chi(T)$. DERIVATION OF EQUATIONS 1-4 IN THE ARTICLE

PROOF OF EQ. 1 IN THE ARTICLE.– Consider a system S that interacts with a bath B. Denote the total density matrix of the composite object as ρ_{total}, and the reduced density matrices for the system and the bath as ρ and ρ_B, respectively. That is, $\rho = \text{Tr}_B\, \rho_{\text{total}}$, where the trace is over the degrees of freedom of the bath, and similarly for ρ_B. Assume that the initial state of ρ_{total} is a tensor product form,

$$\rho_{\text{total}}(0) = \rho(0) \otimes \rho_B(0), \tag{S1}$$

where $\rho_B(0)$ is always

$$\rho_B(0) = \sum_\beta p_\beta |e_\beta\rangle\langle e_\beta|, \tag{S2}$$

for every initial state $\rho(0)$ of the system, with $p_\beta \geq 0$ and $\sum_\beta p_\beta = 1$. At time T, the total state is a unitary evolution of the initial total state,

$$\rho_{\text{total}}(T) = U(T)\rho(0) \otimes \rho_B(0)U^\dagger(T). \tag{S3}$$

Here, $U(T) = \mathcal{T}(e^{-i\int_0^T H_{\text{total}}(t')dt'})$ is the propagator for the entire object, $\mathcal{T}$ is the time-ordering operator, and

$$H_{\text{total}} = H_S + H_B + H_{SB}, \tag{S4}$$

where H_S, H_B, H_{SB} are terms in the Hamiltonian that depend only on degrees of freedom of S, B, or both, respectively. Taking the trace of Eq. S3 with respect to the states of B yields

$$\rho(T) = \sum_{\alpha\beta} p_\beta E_{\alpha\beta}(T)\rho(0)E^\dagger_{\alpha\beta}(T) \tag{S5}$$

where

$$E_{\alpha\beta}(T) = \langle e_\alpha|U(T)|e_\beta\rangle, \tag{S6}$$

is a Kraus operator and Eq. (S5) is known as the *operator sum representation* [1, 2].

By identifying:

$$\begin{aligned}\chi_{abcd}(T) &= \sum_{\alpha\beta}[E_{\alpha\beta}(t)]_{ac}[E^\dagger_{\alpha\beta}(t)]_{db} \\ &= \sum_{\alpha\beta} p_\beta \langle e_\alpha, a|U(T)|e_\beta, c\rangle\langle e_\beta, d|U^+(T)|e_\alpha, b\rangle\end{aligned} \tag{S7}$$

we have proven the equivalence between Eq. S5 and 1 in the article. An important caveat which is clear from the derivation is the following: $\rho_B(0)$ must be the same for every initial state in S for $\chi(T)$ to be well-defined. Also, different states $\rho_B(0)$ will obviously yield different processes. □

PROOF OF EQ. 2 IN THE ARTICLE.– Manipulating Eq. S7, it follows that

$$\begin{aligned}\chi_{badc}(T) &= \sum_{\alpha\beta} p_\beta \langle e_\alpha, b|U(T)|e_\beta, d\rangle\langle e_\beta, c|U^\dagger(T)|e_\alpha, a\rangle \\ &= \left(\sum_{\alpha\beta} p_\beta \langle e_\alpha, a|U(T)|e_\beta, c\rangle\langle e_\beta, d|U^\dagger(T)|e_\alpha, b\rangle\right)^* \\ &= \chi^*_{abcd}(T). \end{aligned} \tag{S8}$$

□

Eq. 2 in the article preserves the Hermiticity of the density matrix.

$$\begin{aligned}\rho_{ba}(T) &= \sum_{cd} \chi_{badc}(T)\rho_{dc}(0) \\ &= \sum_{cd} \chi^*_{abcd}(T)\rho^*_{cd}(0) \\ &= \left[\sum_{cd} \chi_{abcd}(T)\rho_{cd}(0)\right]^* \\ &= \rho^*_{ab}(T). \end{aligned} \tag{S9}$$

PROOF OF EQ. 3 IN THE ARTICLE.– Using Eq. S7, and exploiting the fact that $U(T)U^\dagger(T) = U^\dagger(T)U(T) = I_S \otimes I_B$, the identity on the whole space, we get:

$$\begin{aligned}\sum_a \chi_{aacd}(T) &= \sum_{a\alpha\beta} p_\beta \langle e_\alpha, a|U(T)|e_\beta, c\rangle\langle e_\beta, d|U^\dagger(T)|e_\alpha, a\rangle \\ &= \sum_{a\alpha\beta} p_\beta \langle e_\beta, d|U^\dagger(T)|e_\alpha, a\rangle\langle e_\alpha, a|U(T)|e_\beta, c\rangle \\ &= \sum_{\beta} p_\beta \langle e_\beta, d|e_\beta, c\rangle \\ &= \delta_{cd}. \end{aligned} \tag{S10}$$

□

Eq. 3 in the article preserves the trace of the density matrix:

$$\begin{aligned}\mathrm{Tr}(\rho(T)) &= \sum_{acd} \chi_{aacd}(T)\rho_{cd}(0) \\ &= \sum_{cd} \delta_{cd}\rho_{cd}(0) \\ &= \mathrm{Tr}(\rho(0)). \end{aligned} \tag{S11}$$

PROOF OF EQ. 4 IN THE ARTICLE.– Again, manipulating Eq. S7:

$$\begin{aligned}\sum_{abcd} z^*_{ac}\chi_{abcd}(T)z_{bd} &= \sum_{abcd} z^*_{ac}\sum_{\alpha\beta} p_\beta \langle e_\alpha, a|U(T)|e_\beta, c\rangle\langle e_\beta, d|U^\dagger(T)|e_\alpha, b\rangle z_{bd} \\ &= \sum_{\alpha\beta} p_\beta \zeta_\alpha \zeta^*_\alpha \\ &\geq 0,\end{aligned}$$

where we have defined $\zeta_\alpha = \sum_{ac} z^*_{ac}\langle e_\alpha, a|U(T)|e_\beta, c\rangle$. □.

Suppose $\rho(0)$ is Hermitian positive-semidefinite (HPS), so that we may write $\rho_{cd}(0) = \sum_k U^*_{kc} q_k U_{kd}$ where U is a unitary transformation that diagonalizes $\rho(0)$, and $q_k \geq 0$ for all k. Is the HPS condition maintained for $\rho(T)$? If so, it must satisfy $\sum_{ab} y^*_a \rho_{ab}(T) y_b \geq 0$ for an arbitrary vector y. Eq. 4 in the article guarantees this:

$$\begin{aligned}\sum_{ab} y^*_a \rho_{ab}(T) y_b &= \sum_{abcdk} y^*_a \chi_{abcd}(T) U^*_{kc} q_k U_{kd} y_b \\ &= \sum_k \sum_{abcd} z^{(k)*}_{ac} \chi_{abcd}(T) z^{(k)}_{bd} \\ &\geq 0,\end{aligned}$$

where we have identified the vectors $z^{(k)}$ with elements $z^{(k)}_{bd} = \sqrt{q_k} U_{kd} y_b$.

II. TRANSITION DIPOLES OF THE COUPLED DIMER MODEL

Since we are concerned with the interaction of the chromophores with electromagnetic radiation, we make some remarks on the geometry of the transition dipoles (see Fig. S1). Let the independent site transition dipole moments from the ground to the single exciton be $\boldsymbol{d}_A$ and $\boldsymbol{d}_B$, respectively. The transition dipole moments for the relevant eigenstate transitions are (see for example, [3]):

$$\begin{aligned}\begin{bmatrix}\boldsymbol{\mu}_{\alpha g}\\ \boldsymbol{\mu}_{\beta g}\end{bmatrix} &= \begin{bmatrix}\cos\theta & \sin\theta\\ -\sin\theta & \cos\theta\end{bmatrix}\begin{bmatrix}\boldsymbol{d}_A\\ \boldsymbol{d}_B\end{bmatrix} \\ \begin{bmatrix}\boldsymbol{\mu}_{f\alpha}\\ \boldsymbol{\mu}_{f\beta}\end{bmatrix} &= \begin{bmatrix}\sin\theta & \cos\theta\\ \cos\theta & -\sin\theta\end{bmatrix}\begin{bmatrix}\boldsymbol{d}_A\\ \boldsymbol{d}_B\end{bmatrix}.\end{aligned} \tag{S12}$$

To simplify notation, we assume that $J \neq 0$ and the components of $\boldsymbol{d}_A$ and $\boldsymbol{d}_B$ are all real, which imply that $\boldsymbol{\mu}_{ij} = \boldsymbol{\mu}_{ji}$, for all $i, j \in \{\alpha, \beta, f\}$. For a coupled heterodimer, the four dipoles in Eq. (S12) are located in the same plane, but in general have different magnitudes

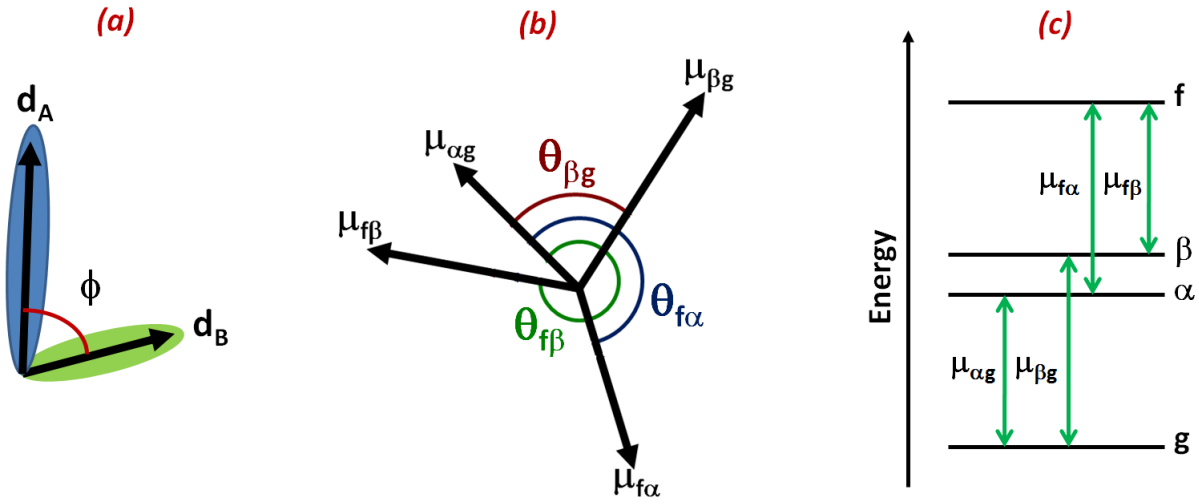

Figure S1: *Parameters of the coupled heterodimer.* (a) Dipole vectors $\boldsymbol{d}_A$ and $\boldsymbol{d}_B$ for each chromophoric site. The angle between them is ϕ. (b) Transition dipole moments between the different eigenstates of H_S; angles are referenced with respect to $\boldsymbol{\mu}_{\alpha g}$. (c) Energy spectrum of H_S and allowed dipole transitions.

and directions. We label the magnitude of $\boldsymbol{\mu}_{ij}$ with μ_{ij} and the angle between $\boldsymbol{\mu}_{ij}$ and $\boldsymbol{\mu}_{\alpha g}$ with ϕ_{ij}, so that the reference is with respect to $\theta_{\alpha g} = 0$ (Fig. S1).

The different transition dipole moments can be easily expressed in terms of the angle ϕ between $\boldsymbol{d}_A$ and $\boldsymbol{d}_B$, and the mixing angle θ. We present these functional dependences for completeness. We define our coordinate axes so

$$\begin{aligned} \boldsymbol{d}_A &= d_A \hat{z}, \\ \boldsymbol{d}_B &= (d_B \cos\phi)\hat{z} + (d_B \sin\phi)\hat{x}. \end{aligned} \tag{S13}$$

We can expressing the components of the transition dipole moments,

$$\begin{aligned} \boldsymbol{\mu}_{\alpha g} &= (d_B \sin\theta \sin\phi)\hat{x} + (d_A \cos\theta + d_B \sin\theta \cos\phi)\hat{z}, \\ \boldsymbol{\mu}_{\beta g} &= (d_B \cos\theta \sin\phi)\hat{x} + (-d_A \sin\theta + d_B \cos\theta \cos\phi)\hat{z}, \\ \boldsymbol{\mu}_{f\alpha} &= (d_B \cos\theta \sin\phi)\hat{x} + (d_A \sin\theta + d_B \cos\theta \cos\phi)\hat{z}, \\ \boldsymbol{\mu}_{f\beta} &= (-d_B \sin\theta \sin\phi)\hat{x} + (d_A \cos\theta - d_B \sin\theta \cos\phi)\hat{z}. \end{aligned} \tag{S14}$$

The angles between the different transition dipole moments can be calculated as

$$\begin{aligned} \cos(\phi_{ij}) &= \frac{\boldsymbol{\mu}_{\alpha g} \cdot \boldsymbol{\mu}_{ij}}{\mu_{\alpha g}\mu_{ij}}, \\ \sin(\phi_{ij}) &= \frac{|\boldsymbol{\mu}_{\alpha g} \times \boldsymbol{\mu}_{ij}|}{\mu_{\alpha g}\mu_{ij}}. \end{aligned} \tag{S15}$$

where μ_{ij} denotes the norm of the respective dipole. For a homodimer with $\theta = \frac{\pi}{4}$, $d_A = d_B$ and $\boldsymbol{\mu}_{f\alpha} = \boldsymbol{\mu}_{\alpha g}$, $\boldsymbol{\mu}_{f\beta} = -\boldsymbol{\mu}_{\beta g}$, yielding only two independent directions for the four transition dipoles [4]. For a homodimer with $\theta = \frac{3\pi}{4}$, the conclusion is similar.

III. STATE PREPARATION. DERIVATION OF EQUATION (9) IN THE ARTICLE

The second order density matrix in λ that results after considering the components of the first two pulses at $-\boldsymbol{k}_1$ and $+\boldsymbol{k}_2$ can be calculated in Liouville space as (see [5]),

$$\begin{aligned}
&\tilde{\rho}^{\omega_1,\omega_2}_{\boldsymbol{e}_1,\boldsymbol{e}_2}(t_2+T) \\
&= \left(\frac{1}{i}\right)^2 \int_{-\infty}^{t_2+T} dt'' \int_{-\infty}^{t''} dt' \mathcal{G}_2(t_2+T,t'')\tilde{\mathcal{V}}(t'')\mathcal{G}_1(t'',t')\tilde{\mathcal{V}}(t')\rho(-\infty),
\end{aligned} \tag{S16}$$

where $\rho(-\infty) = |g\rangle\langle g|$, or alternatively, in Liouville space notation, $\rho(-\infty) = |gg\rangle\rangle$, is the state of the system before the perturbations. We are interested in the situation $T > 3\sigma$, that is, after the action of the two pulses has practically ceased. The perturbation superoperator is $\tilde{\mathcal{V}}(t) = \sum_{i=1}^{3} \tilde{\mathcal{V}}_i(t)$, where $\tilde{\mathcal{V}}_i(t) = [\tilde{V}_i, \cdot]$, and

$$\begin{aligned}
\tilde{V}_1(t) &= -\lambda \hat{\boldsymbol{\mu}}^{<} \cdot \boldsymbol{e_1} E(t-t_1) e^{i\omega_1(t-t_1)} \\
\tilde{V}_2(t) &= -\lambda \hat{\boldsymbol{\mu}}^{>} \cdot \boldsymbol{e_2} E(t-t_2) e^{-i\omega_2(t-t_2)} \\
\tilde{V}_3(t) &= -\lambda \hat{\boldsymbol{\mu}}^{>} \cdot \boldsymbol{e_3} E(t-t_3) e^{-i\omega_3(t-t_3)}.
\end{aligned} \tag{S17}$$

These expressions conveniently adapt Eq. 6 in the article to account for the phase matching direction of $\boldsymbol{k}_{PE}$ and to consider the RWA, where $\hat{\boldsymbol{\mu}}^{<} = \sum_{\omega_p<\omega_q} \boldsymbol{\mu}_{pq}|p\rangle\langle q|$ promotes emissions from the ket or absorptions on the bra, and $\hat{\boldsymbol{\mu}}^{>} = (\hat{\boldsymbol{\mu}}^{<})^{+}$ induces the opposite processes.

A. Well separated pulses 1 and 2

We can simplify Eq. S16 by considering that: (a) if $\tau > 3\sigma$, the pulses are well separated, and we can perform the substitution $\tilde{\mathcal{V}}(t') = \tilde{\mathcal{V}}_1(t')$ and $\tilde{\mathcal{V}}(t'') = \tilde{\mathcal{V}}_2(t'')$; (b) we focus only on the dominant contribution due to the resonant transitions. As mentioned in the text, this calculation can be easily grasped by analyzing the double-sided Feynman diagrams in Fig. 2a–d. Since we are looking for signals only in the direction $-\boldsymbol{k}_1 + \boldsymbol{k}_2 + \boldsymbol{k}_3$, the first pulse must interact via the operator $\hat{\boldsymbol{\mu}}^{<}$, so it can only act on the bra to produce optical coherences $|gp\rangle\rangle$. We assume that these coherences evolve unitarily together with a constant dephasing rate (this assumption is not necessary, but it simplifies our analysis):

$$\begin{aligned}
\mathcal{G}_1(t'',t') &= \mathcal{G}(t''-t') \\
&= \sum_{mn} \mathcal{G}_{mn}(t''-t')|mn\rangle\rangle\langle\langle mn|,
\end{aligned} \tag{S18}$$

where $\mathcal{G}_{mn}(\tau)$ is given by Eq. 11 in the article. The second pulse can act on the ket to create the coherence $|pq\rangle\rangle$ if $p \neq q$. However, in case the frequency component of the second pulse is the same as that of the first pulse, it can excite the ket to form a population $|qq\rangle\rangle$ or de-excite the bra to go back to $-|gg\rangle\rangle$ (with opposite sign due to the commutator). For the evolution in the waiting time, we use the following identity:

$$\mathcal{G}_2(t_2+T,t'') \;=\; \chi(T)\mathcal{G}(t_2-t''), \tag{S19}$$

where we have formally introduced the process matrix $\chi(T)$ acting as the propagator after time t_2. Altogether, we have in Liouville space a perturbation, a free evolution, another perturbation, and free evolution. The effective second order density matrix associated with the perturbations at $-\boldsymbol{k}_1+\boldsymbol{k}_2$ is given by:

$$\begin{aligned}
&\tilde{\rho}^{\omega_1,\omega_2}_{\boldsymbol{e}_1,\boldsymbol{e}_2}(t_2+T)\\
=\; &-\left(\frac{-\lambda}{i}\right)^2\sum_{pq}\Bigg[\int_{-\infty}^{t_2+T}dt''\chi(T)\Big\{\mathcal{G}_{qp}(t_2-t'')\left(\boldsymbol{\mu}_{qg}\cdot\boldsymbol{e}_2|q\rangle\langle g|E(t''-t_2)e^{-i\omega_2(t''-t_2)}\right)\\
&\times\int_{-\infty}^{t''}dt'\mathcal{G}_{gp}(t''-t')|g\rangle\langle g|\left(|g\rangle\langle p|\boldsymbol{\mu}_{pg}\cdot\boldsymbol{e}_1E(t'-t_1)e^{i\omega_1(t'-t_1)}\right)\Big\}\\
&-\int_{-\infty}^{t_2+T}dt''\chi(T)\Big\{\mathcal{G}_{gg}(t_2-t'')\\
&\times\int_{-\infty}^{t''}dt'\mathcal{G}_{gp}(t''-t')|g\rangle\langle g|\left(|g\rangle\langle p|\boldsymbol{\mu}_{pg}\cdot\boldsymbol{e}_1E(t'-t_1)e^{i\omega_1(t'-t_1)}\right)\\
&\times\left(|q\rangle\langle g|\boldsymbol{\mu}_{qg}\cdot\boldsymbol{e}_2E(t''-t_2)e^{i\omega_1(t''-t_2)}\right)\Big\}\Bigg]
\end{aligned} \tag{S20}$$

This calculation is a double integral over all the possible times t' and t'' in which the perturbations due to the pulses at $-\boldsymbol{k}_1$ and $+\boldsymbol{k}_2$ can act due to their finite width σ. The time-ordering consideration is unimportant for $\tau, T \gg \sigma$, and in fact, both integrals can be extended to the entire real space: $\int_{-\infty}^{t_2+T}dt''\int_{-\infty}^{t''}dt'(\cdot) \approx \int_{-\infty}^{\infty}dt''\int_{-\infty}^{\infty}dt'(\cdot)$. As discussed in the next subsection, the approximation $T \gg \sigma$ is needed (so that the pulse envelopes are nearly zero at time t_2+T), but the $\tau \gg \sigma$ assumption is unnecessary. We then rewrite

$$\begin{aligned}
\approx\; &-\left(\frac{-\lambda}{i}\right)^2\sum_{pq}(\boldsymbol{\mu}_{pg}\cdot\boldsymbol{e}_1)(\boldsymbol{\mu}_{qg}\cdot\boldsymbol{e}_2)\\
&\times\int_{-\infty}^{\infty}d(t'-t_1)\left(\mathcal{G}_{gp}(t_1-t')E(t'-t_1)e^{i\omega_1(t'-t_1)}\right)\\
&\times\chi(T)\Big\{\int_{-\infty}^{\infty}d(t_2-t'')\mathcal{G}_{qp}(t_2-t'')E(t''-t_2)e^{-i\omega_2(t''-t_2)}\mathcal{G}_{gp}(t''-t_2)|q\rangle\langle p|\\
&-\delta_{pq}(\mathcal{G}_{gg}(t_2-t'')E(t''-t_2)e^{-i\omega_2(t''-t_2)}\mathcal{G}_{gp}(t''-t_2)|g\rangle\langle g|)\Big\}
\end{aligned} \tag{S21}$$

The length of the pulse σ is much shorter than the dynamics induced by the bath. Therefore, $\sigma \ll \frac{1}{\Gamma_{mn}}$, and dephasing contributions can be neglected within the integral so that $\mathcal{G}_{gp}(t_1-t') \approx e^{i\omega_{pg}(t_1-t')}$, $\mathcal{G}_{qp}(t_2-t'')\mathcal{G}_{gp}(t''-t_2) \approx e^{-i\omega_{qp}(t_2-t'')}e^{i\omega_{pg}(t_2-t'')} = e^{-i\omega_{qg}(t_2-t'')}$, and $\mathcal{G}_{gp}(t''-t_2) \approx e^{-i\omega_{pg}(t''-t_2)}$, $\mathcal{G}_{gg}(t''-t_2) \approx e^{-i\omega_{gg}(t''-t_2)}$. However, the dephasing terms are non-negligible in the free evolution between the pulses if $\tau \gg \sigma$, and the term $\mathcal{G}_{gp}(\tau)$ in the final expression cannot in general be simplified to $e^{-i\omega_{gp}\tau}$. Then we have

$$\begin{aligned}
&\approx -\left(\frac{-\lambda}{i}\right)^2 \sum_{pq} (\boldsymbol{\mu}_{pg}\cdot\boldsymbol{e}_1)(\boldsymbol{\mu}_{qg}\cdot\boldsymbol{e}_2) \int_{-\infty}^{\infty} ds' e^{-i\omega_{pg}s'} E(s') e^{i\omega_1 s'} \int_{-\infty}^{\infty} ds'' e^{i\omega_{pg}s''} \\
&\quad \times\chi(T)\left\{E(s'')e^{-i\omega_2 s''}(|q\rangle\langle p| - \delta_{pq}|g\rangle\langle g|)\right\} \\
&= -\chi(T)\left\{\sum_{pq} C^p_{\omega_1} C^q_{\omega_2} (\boldsymbol{\mu}_{pg}\cdot\boldsymbol{e}_1)(\boldsymbol{\mu}_{qg}\cdot\boldsymbol{e}_2)\mathcal{G}_{gp}(t_2-t_1)(|q\rangle\langle p| - \delta_{pq}|g\rangle\langle g|)\right\}, \qquad \text{(S22)}
\end{aligned}$$

The final result has a clear physical interpretation: Each of the transitions depicted in the diagrams in Fig. 2a-d is controlled by the frequency components of the pulse at the given transition (terms $C^p_{\omega_1}$ and $C^q_{\omega_2}$), as well as the alignment between the transition dipole and the pulse polarization. Free evolution of the optical coherence between the perturbations is given by $\mathcal{G}_{gp}(\tau)$. Once the state $|q\rangle\langle p| - \delta_{pq}|g\rangle\langle g|$ is formed, the superoperator $\chi(T)$ acts on it, encoding both coherent and dissipative processes.

B. Overlapping pulses 1 and 2

We now consider $0 \leq \tau < 3\sigma$. Eq. (9) in the article rigorously holds for this more general case. For the contribution due to the original diagrams in Fig. 2a–d, we carry out the same double integral of Eq. (S20), but we keep it time ordered as $\int_{-\infty}^{\infty} dt'' \int_{-\infty}^{t''} dt'(\cdot)$. Additionally, each diagram in Fig. 2a–d corresponds to another diagram where the pulse at $+\boldsymbol{k}_2$ acts before the one at $-\boldsymbol{k}_1$, but yields back the same state after the two pulses (for example, the one corresponding to Fig. 2b would be $gg \to \beta g \to \beta\alpha$). Their contributions to $[\rho^{(2)}_{-\boldsymbol{k}_1,\boldsymbol{k}_2}]^{\omega_1,\omega_2}_{\boldsymbol{e}_1,\boldsymbol{e}_2}(t_2+T)$ can be easily shown to be $\int_{-\infty}^{\infty} dt'' \int_{t''}^{\infty} dt'(\cdot)$, where the integrand and the dummy variable convention are the same as before. The sum of the two contributions yields back the double integral as in Eq. (S21).

IV. STATE DETECTION. DERIVATION OF EQUATIONS 14-16 IN THE ARTICLE

The techniques to derive these equations are the same as the ones used for the previous section. However, the proliferation of terms makes the full exposition of the derivation unwieldy. Therefore, we only illustrate how some sample terms arise.

A. Well separated pulses 3 and 4

Let us start by noting that, using Eq. (9) in the article, the element ij of $\tilde{\rho}^{\omega_1,\omega_2}_{\boldsymbol{e}_1,\boldsymbol{e}_2}(t_2+T)$ can be expressed as:

$$\begin{aligned}
&\langle i|\tilde{\rho}^{\omega_1,\omega_2}_{\boldsymbol{e}_1,\boldsymbol{e}_2}(t_2+T)|j\rangle \\
&\left\langle i\left|-\chi(T)\left\{\sum_{pq} C^p_{\omega_1} C^q_{\omega_2}(\boldsymbol{\mu}_{pg}\cdot\boldsymbol{e}_1)(\boldsymbol{\mu}_{qg}\cdot\boldsymbol{e}_2)\mathcal{G}_{gp}(\tau)(|q\rangle\langle p|-\delta_{pq}|g\rangle\langle g|)\right\}\right|j\right\rangle \\
=\ &-\sum_{pq} C^p_{\omega_1} C^q_{\omega_2}(\boldsymbol{\mu}_{pg}\cdot\boldsymbol{e}_1)(\boldsymbol{\mu}_{qg}\cdot\boldsymbol{e}_2)\mathcal{G}_{gp}(\tau)(\chi_{ijqp}(T)-\delta_{pq}\delta_{ij}\delta_{ig}).
\end{aligned} \tag{S23}$$

We define $[\rho^{(3)}_{-\boldsymbol{k}_1,\boldsymbol{k}_2,\boldsymbol{k}_3}]^{\omega_1,\omega_2,\omega_3}_{\boldsymbol{e}_1,\boldsymbol{e}_2,\boldsymbol{e}_3}(t_3+t)$ analogously to the way $\tilde{\rho}^{\omega_1,\omega_2}_{\boldsymbol{e}_1,\boldsymbol{e}_2}(t_2+T)$ was defined in Eq. (S16), that is, the third-order in λ density matrix due to the perturbations corresponding to the phase-matching direction $-\boldsymbol{k}_1+\boldsymbol{k}_2+\boldsymbol{k}_3$. For $t\gg\sigma$, we can easily calculate the matrix elements of $[\rho^{(3)}_{-\boldsymbol{k}_1,\boldsymbol{k}_2,\boldsymbol{k}_3}]^{\omega_1,\omega_2,\omega_3}_{\boldsymbol{e}_1,\boldsymbol{e}_2,\boldsymbol{e}_3}(t_3+t)$ that yield an optical dipole, say αg, and can then find the contribution of the latter to the polarization via trace with respect to $\hat{\boldsymbol{\mu}}$ (see Fig. 2e and h):

$$\begin{aligned}
&\mathrm{Tr}(\hat{\boldsymbol{\mu}}\langle\alpha|[\rho^{(3)}_{-\boldsymbol{k}_1,\boldsymbol{k}_2,\boldsymbol{k}_3}]^{\omega_1,\omega_2,\omega_3}_{\boldsymbol{e}_1,\boldsymbol{e}_2,\boldsymbol{e}_3}(t_3+t)|g\rangle|\alpha\rangle\langle g|) \\
=\ &-\mathrm{Tr}[\hat{\boldsymbol{\mu}}\sum_{pq} C^p_{\omega_1} C^q_{\omega_2}(\boldsymbol{\mu}_{pg}\cdot\boldsymbol{e}_1)(\boldsymbol{\mu}_{qg}\cdot\boldsymbol{e}_2)\mathcal{G}_{gp}(\tau) \\
&\times\left(\frac{-\lambda}{i}\right)\int_{-\infty}^{t_3+t} dt'\mathcal{G}_{\alpha g}(t_3+t-t')E(t'-t_3)e^{-i\omega_3(t'-t_3)} \\
&\times\{\left(\boldsymbol{\mu}_{\alpha g}\cdot\boldsymbol{e}_3|\alpha\rangle\langle g|\right)\left(e^{-i\omega_{gg}(t'-t_3)}\left(\chi_{ggqp}(T)-\delta_{pq}\right)|g\rangle\langle g|\right) \\
&-\left(e^{-i\omega_{\alpha\alpha}(t'-t_3)}\chi_{\alpha\alpha qp}(T)|\alpha\rangle\langle\alpha|\right)\left(|\alpha\rangle\langle g|\boldsymbol{\mu}_{\alpha g}\cdot\boldsymbol{e}_3\right) \\
&-\left(e^{-i\omega_{\alpha\beta}(t'-t_3)}\chi_{\alpha\beta qp}(T)|\alpha\rangle\langle\beta|\right)\left(|\beta\rangle\langle g|\boldsymbol{\mu}_{\beta g}\cdot\boldsymbol{e}_3\right)\}] \\
\approx\ &-\sum_{pq} C^p_{\omega_1} C^q_{\omega_2}(\boldsymbol{\mu}_{pg}\cdot\boldsymbol{e}_1)(\boldsymbol{\mu}_{qg}\cdot\boldsymbol{e}_2)\mathcal{G}_{gp}(\tau) \\
&\times\{C^\alpha_{\omega_3}(\boldsymbol{\mu}_{\alpha g}\cdot\boldsymbol{e}_3)\mathcal{G}_{\alpha g}(t)(\chi_{ggqp}(T)-\delta_{pq}-\chi_{\alpha\alpha qp}(T)) \\
&-C^\beta_{\omega_3}(\boldsymbol{\mu}_{\beta g}\cdot\boldsymbol{e}_3)\mathcal{G}_{\alpha g}(t)\chi_{\alpha\beta qp}(T)\}\boldsymbol{\mu}_{\alpha g},
\end{aligned} \tag{S24}$$

where, just as before, we have used the fact that $\sigma\ll\frac{1}{\Gamma_{\alpha g}}$ to approximate that $\mathcal{G}_{\alpha g}(t_3+t-t')\approx\mathcal{G}_{\alpha g}(t)e^{i\omega_{\alpha g}(t'-t_3)}$, and the integrals have been extended to the entire real axis. The third pulse at $+\boldsymbol{k}_3$ can excite the ket or de-excite the bra of the output state at the waiting time. The calculation above simply enumerates the resonant transitions $gg,\alpha\alpha,\alpha\beta\to\alpha g$ due to the laser components associated with $C^\alpha_{\omega_3}$, $C^\alpha_{\omega_3}$, and $C^\beta_{\omega_3}$, respectively, and takes the trace of the optical coherence with respect to the dipole operator: $\mathrm{Tr}(\hat{\boldsymbol{\mu}}|\alpha\rangle\langle g|)=\boldsymbol{\mu}_{\alpha g}$. Recall that we have chosen the dipole elements to be purely real.

The detection of the polarization due to the αg coherence occurs through heterodyning. The fourth ultrashort pulse interferes with the coherence oscillating as $e^{i\omega_{\alpha g}(t''-t_4)}$, yielding a contribution to the time integrated signal encoded by:

$$\begin{aligned}
&\int_{-\infty}^{\infty} dt'' e^{i\omega_4(t''-t_4)} E(t''-t_4) e^{-i\omega_{\alpha g}(t''-t_4)} \\
=\ & i\sqrt{2\pi\sigma^2} e^{-\sigma^2(\omega_{\alpha g}-\omega_4)^2/2} \\
\propto\ & C^{\alpha}_{\omega_4}.
\end{aligned} \tag{S25}$$

In words, the Fourier components of the fourth pulse filter the optical coherences of the polarization associated sample. In our case, the polarization due to the coherence αg will be detected as $C^{\alpha}_{\omega_4}$, that is, proportionally to the frequency component of the fourth pulse at $\omega_{\alpha g}$. Altogether, the calculation reads:

$$\begin{aligned}
&\int_{-\infty}^{\infty} e^{i\omega_4(t''-t_4)} E(t''-t_4) e^{-i\omega_{\alpha g}(t''-t_4)} \\
&\times \boldsymbol{e_4} \cdot \mathrm{Tr}(\hat{\boldsymbol{\mu}} \langle \alpha | [\rho^{(3)}_{-\boldsymbol{k}_1,\boldsymbol{k}_2,\boldsymbol{k}_3}]^{\omega_1,\omega_2,\omega_3}_{\boldsymbol{e}_1,\boldsymbol{e}_2,\boldsymbol{e}_3}(t_3+t) |g\rangle |\alpha\rangle\langle g|) \\
\propto\ & C^{\alpha}_{\omega_4} \boldsymbol{e}_4 \cdot \mathrm{Tr}(\hat{\boldsymbol{\mu}} \langle \alpha | [\rho^{(3)}_{-\boldsymbol{k}_1,\boldsymbol{k}_2,\boldsymbol{k}_3}]^{\omega_1,\omega_2,\omega_3}_{\boldsymbol{e}_1,\boldsymbol{e}_2,\boldsymbol{e}_3}(t_3+t) |g\rangle |\alpha\rangle\langle g|) \\
=\ & -\sum_{pq} C^{p}_{\omega_1} C^{q}_{\omega_2} (\boldsymbol{\mu}_{pg} \cdot \boldsymbol{e}_1)(\boldsymbol{\mu}_{qg} \cdot \boldsymbol{e}_2) \mathcal{G}_{gp}(\tau) \\
&\times \{ C^{\alpha}_{\omega_3} C^{\alpha}_{\omega_4} (\boldsymbol{\mu}_{\alpha g} \cdot \boldsymbol{e}_3)(\boldsymbol{\mu}_{\alpha g} \cdot \boldsymbol{e}_4) \mathcal{G}_{\alpha g}(t) (\chi_{ggqp}(T) - \delta_{pq} - \chi_{\alpha\alpha qp}(T)) \\
&- C^{\beta}_{\omega_3} C^{\alpha}_{\omega_4} (\boldsymbol{\mu}_{\beta g} \cdot \boldsymbol{e}_3)(\boldsymbol{\mu}_{\alpha g} \cdot \boldsymbol{e}_4) \mathcal{G}_{\alpha g}(t) \chi_{\alpha\beta qp}(T) \}.
\end{aligned} \tag{S26}$$

This exercise can be repeated for the rest of the optical coherences which occur in the echo time and yield detectable dipoles: $\beta g, f\alpha, f\beta$ (Fig. 2-e,f,g,h). The total signal is

$$\begin{aligned}
&[S_{PE}]^{\omega_1,\omega_2,\omega_3,\omega_4}_{\boldsymbol{e}_1,\boldsymbol{e}_2,\boldsymbol{e}_3,\boldsymbol{e}_4}(\tau,T,t) \\
=\ & \sum_{uv=\alpha g,\beta g,f\alpha,f\beta} \int_{-\infty}^{\infty} dt'' e^{i\omega_4(t''-t_4)} E(t''-t_4) e^{-i\omega_{ij}(t''-t_4)} \\
&\times \boldsymbol{e_4} \cdot \mathrm{Tr}(\hat{\boldsymbol{\mu}} \langle u | [\rho^{(3)}_{-\boldsymbol{k}_1,\boldsymbol{k}_2,\boldsymbol{k}_3}]^{\omega_1,\omega_2,\omega_3}_{\boldsymbol{e}_1,\boldsymbol{e}_2,\boldsymbol{e}_3}(t_3+t) |v\rangle |u\rangle\langle v|),
\end{aligned} \tag{S27}$$

which yields Eq. 14 in the article. That equation has been rewritten by grouping the terms in the forms of Eqs. 15 and 16 in the article, and their analogues upon the $\alpha, \beta \to \beta, \alpha$ substitutions in order to classify the processes corresponding to the frequencies of the transition due to the third pulse and the heterodyne detection.

B. Overlapping pulses 3 and 4

We now consider $0 \leq t$ rather than $3\sigma < t$, to consider overlapping pulses 3 and 4. Eq. 14 in the article must be slightly modified when the overlap in time between the third and the fourth pulses is significant. As opposed to Section III-B of this Appendix, where the first pulse can act on the system before the second pulse *and* viceversa, in the detection stage, the third pulse must act on the system to yield a polarization *before* the fourth pulse (which does not interact with the system) can detect it. Hence, the LO cannot be regarded on the same footing as the other three pulses.

First, we state the solution to the relevant integral:

$$\begin{aligned}
&\int_{-\infty}^{\infty} dt'' \int_{-\infty}^{t''} dt' e^{i\omega_4(t''-t_4)} E(t''-t_4) e^{-i\omega_{uv}(t''-t_4)} \mathcal{G}_{uv}(t) e^{i\omega_{uv}(t'-t_3)} E(t'-t_3) e^{-i\omega_3(t'-t_3)} e^{-i\omega_{ij}(t'-t_3)} \\
&= \left(\sqrt{\pi\sigma^2} e^{-(\omega_3-(\omega_{uv}-\omega_{ij}))^2\sigma^2/2}\right)\left(\sqrt{\pi\sigma^2} e^{-(\omega_4-(\omega_4-\omega_{uv}))^2}\right) \\
&\quad \times \left(1 + Erf\left(\frac{t}{2\sigma} + \frac{(\omega_3-(\omega_{uv}-\omega_{ij})+\omega_4-\omega_{uv})\sigma}{2}\right)\right) \mathcal{G}_{uv}(t), \qquad \text{(S28)}
\end{aligned}$$

which applies to the $ij \to uv$ transition caused by the third pulse at $+\boldsymbol{k}_3$, followed by an effective free evolution $\mathcal{G}_{uv}(t)$ for the echo interval $t = t_4 - t_3$, and the detection of the optical coherence uv via the LO. Importantly, the upper limit of the integral over t', associated with the action of the third pulse, cannot be taken to ∞, since the LO may interfere with the transients of the polarization before the envelope of the third pulse is effectively over. There is no contribution from the complementary integral going from t'' to ∞ since the LO is assumed not to interact with the system and, hence, does not contribute to the polarization of the sample.

Repeating the derivation of Eq. S24 by not taking the upper limit of the t'' integral to ∞, it can be seen that the only modification to Eq. 14 in the article is given by Eq. 17 in the article. That is, the amplitudes of the third transition and the action of the LO are correlated by an error function. In the limiting case when $t \gg \sigma$, Eq. 17 recovers $C^r_{\omega_3} C^s_{\omega_4}$, since $Erf(x) \to 1$ as $\Re\{x\} \to \infty$.

V. OVERALL MULTIPLICATIVE CONSTANT

Overall multiplicative constant. Eq. (14) in the article is defined up to a proportionality constant which depends on many factors such as the concentration of the molecules in the experimental sample and the efficiency of the mirrors in the optical setup. This factor may be determined by performing the extraction of $\chi(T)$ up to that constant, and then normalizing

it by enforcing the trace preservation condition of Eq. 3 in the article to hold for population initial states, $c = d$.

VI. ISOTROPIC AVERAGES

The probed sample is an ensemble of isotropically distributed molecules in solution. The isotropic average $\langle\cdot\rangle$ for a tetradic $(\boldsymbol{\mu}_a \cdot \boldsymbol{e}_1)(\boldsymbol{\mu}_b \cdot \boldsymbol{e}_2)(\boldsymbol{\mu}_c \cdot \boldsymbol{e}_3)(\boldsymbol{\mu}_d \cdot \boldsymbol{e}_4)$ is given by [6]:

$$\begin{aligned} &\langle(\boldsymbol{\mu}_a \cdot \boldsymbol{e}_1)(\boldsymbol{\mu}_b \cdot \boldsymbol{e}_2)(\boldsymbol{\mu}_c \cdot \boldsymbol{e}_3)(\boldsymbol{\mu}_d \cdot \boldsymbol{e}_4)\rangle_{iso} \\ = &\sum_{m_1 m_2 m_3 m_4} I^{(4)}_{e_1 e_2 e_3 e_4; m_1 m_2 m_3 m_4} \\ &\times[(\boldsymbol{\mu}_a \cdot \boldsymbol{m}_1)(\boldsymbol{\mu}_b \cdot \boldsymbol{m}_2)(\boldsymbol{\mu}_c \cdot \boldsymbol{m}_3)(\boldsymbol{\mu}_d \cdot \boldsymbol{m}_4)], \end{aligned} \tag{S29}$$

where the isotropically invariant tensor is given by,

$$\begin{aligned} &I^{(4)}_{e_1 e_2 e_3 e_4; m_1 m_2 m_3 m_4} \\ = &\frac{1}{30}\left[\delta_{e_1 e_2}\delta_{e_3 e_4} \;\; \delta_{e_1 e_3}\delta_{e_2 e_4} \;\; \delta_{e_1 e_4}\delta_{e_2 e_3}\right] \\ &\times \begin{bmatrix} 4 & -1 & -1 \\ -1 & 4 & -1 \\ -1 & -1 & 4 \end{bmatrix} \begin{bmatrix} \delta_{m_1 m_2}\delta_{m_3 m_4} \\ \delta_{m_1 m_3}\delta_{m_2 m_4} \\ \delta_{m_1 m_4}\delta_{m_2 m_3} \end{bmatrix}. \end{aligned} \tag{S30}$$

Here, $\boldsymbol{e}_i$ and $\boldsymbol{m}_i$ are the polarizations of the pulses in the lab and the molecular frame, respectively. The isotropic average consists of a sum of molecular frame products $[(\boldsymbol{\mu}_a \cdot \boldsymbol{m}_1)(\boldsymbol{\mu}_b \cdot \boldsymbol{m}_2)(\boldsymbol{\mu}_c \cdot \boldsymbol{m}_3)(\boldsymbol{\mu}_d \cdot \boldsymbol{m}_4)]$ weighted by $I^{(4)}_{e_1 e_2 e_3 e_4; m_1 m_2 m_3 m_4}$. Via this procedure, Eq. 14 in the article becomes:

$$\langle[S_{PE}]^{\omega_1,\omega_2,\omega_3,\omega_4}_{\boldsymbol{e}_1,\boldsymbol{e}_2,\boldsymbol{e}_3,\boldsymbol{e}_4}(\tau,T,t)\rangle_{iso} = \sum_{p,q,r} C^p_{\omega_1} C^q_{\omega_2} C^r_{\omega_3} C^s_{\omega_4} \langle P^{p,q,r,s}_{\boldsymbol{e}_1,\boldsymbol{e}_2,\boldsymbol{e}_3,\boldsymbol{e}_4}(\tau,T,t)\rangle_{iso}. \tag{S31}$$

Due to the structure of Eq. S30, there are signals which vanish in isotropic conditions even though they are finite otherwise. An interesting consequence of this fact is that QPT is not fully realizable for homodimers, since coherence to population and the reverse processes cannot be detected under isotropic conditions [4].

VII. ERRORS IN STATE PREPARATION AND DETECTION

Nontrivial bath-induced dynamics during the coherence or echo times could decrease the robustness of the QPT. Such dynamics manifest as deviations from Eq. (11) in the article and

could be diagnosed by analyzing the signal $[S_{PE}]^{\omega_1,\omega_2,\omega_3,\omega_4}_{\boldsymbol{e}_1,\boldsymbol{e}_2,\boldsymbol{e}_3,\boldsymbol{e}_4}(\tau,T,t)$ collected as a function of τ, with fixed T and t values, or alternatively, by varying t with τ, t fixed. A detailed study of this possibility will be presented elsewhere. Similarly, if the bath evolves away from its equilibrium configuration during the coherence time, with dynamics dependent on the excitonic state, then the initial state for QPT will not be well-defined. This problem can be avoided by taking $\tau = t = 0$ (TD/TB experiments) as described in the article and in the next point.

VIII. DISCUSSION OF THE FACTORIZABLE CONDITION AT $T = 0$

The factorized initial condition assumption in Eq. S1 requires some further discussion. Does it hold for excitonic systems? At $t = -\infty$, we can safely assume that $\rho_{\text{total}}(t = -\infty) = |g\rangle\langle g| \otimes \rho_{B,eq}$, where $\rho_{B,eq}$ is an incoherent ensemble of phonons at thermal equilibrium, and the system state is in the ground electronic state. However, this is not the initial state we are concerned with for a QPT in the single exciton manifold. The state we shall worry about is the one after two pulse perturbations.

First, consider the $\tau = 0$ case (TB and TD experiments). The discussion in Sections III and IV on overlapping pulses is particularly relevant for this situation. Denote $[\rho^{(2)}_{total,-\boldsymbol{k}_1,\boldsymbol{k}_2}]^{\omega_1,\omega_2}_{\boldsymbol{e}_1,\boldsymbol{e}_2}(t_2+T)$ the total second order density matrix corresponding to the perturbations at the $-\boldsymbol{k}_1$ and $+\boldsymbol{k}_2$ directions, such that its trace over the bath yields the object $\tilde{\rho}^{\omega_1,\omega_2}_{\boldsymbol{e}_1,\boldsymbol{e}_2}(t_2+T)$ defined in Eq. 9 in the article. We are interested in the quasi-impulsive limit of the light-matter interaction, where $\sigma \ll \frac{1}{\lambda}$, where σ is the duration of the pulses and λ is the characteristic reorganization energy scale of the bath. As mentioned in the article, in accordance with the Franck-Condon principle, we assume the electronic excitation occurs much faster than any nuclei rearrangement, and $[\rho^{(2)}_{total,-\boldsymbol{k}_1,\boldsymbol{k}_2}]^{\omega_1,\omega_2}_{\boldsymbol{e}_1,\boldsymbol{e}_2}(t_2+T) \approx \tilde{\rho}^{\omega_1,\omega_2}_{\boldsymbol{e}_1,\boldsymbol{e}_2}(t_2+T) \otimes \rho_{B,eq}$, so that Eq. S1 holds.

For $\tau > 0$, the situation needs to be more carefully analyzed. If $\tau \ll \frac{1}{\lambda}$, a similar scenario to the one in the previous paragraph applies (the bath is not given enough time to evolve far away from $\rho_{B,eq}$). Another useful case to consider is $\tau \gg \frac{1}{\lambda}$, after which B relaxes to a stationary or quasi-stationary state $\rho_{B,stat}$, which may or may not be equal to $\rho_{B,eq}$. In order to preserve the factorizable condition, this state $\rho_{B,stat}$ must be the same for every electronic population and coherence of interest, so that $[\rho^{(2)}_{total,-\boldsymbol{k}_1,\boldsymbol{k}_2}]^{\omega_1,\omega_2}_{\boldsymbol{e}_1,\boldsymbol{e}_2}(t_2+T) \approx \tilde{\rho}^{\omega_1,\omega_2}_{\boldsymbol{e}_1,\boldsymbol{e}_2}(t_2+T) \otimes \rho_{B,stat}$. The simplest example of this situation is a Markovian bath, for which B relaxes to $\rho_{B,eq}$ after a timescale on the order of $\frac{1}{\lambda}$, which is short compared to the dynamics of the system.

For cases beyond the ones described here, factorizable initial conditions might not apply, and a reexamination of QPT protocols for initially correlated states must be advocated [7–9]. We are currently pursuing this line of research.

In conclusion, in order to get consistent results for QPT, TD/TB seem to be the most promising experiments. The standard PE experiments with finite τ provide a QPT if the bath is sufficiently "well-behaved," as described above.

IX. TRADING FREQUENCY CONTROL FOR TIME DELAY

Several properties of the pulses can be exploited to selectively manipulate the excitons. These include frequencies [10], polarizations [11–13], and time delays [14–16]. In the article, we have only exploited the former to make a transparent connection between a PE and a QPT experiment. However, the case of polarizations and time delays has also been addressed in our recent work *[4]*. In this section, we address the use of time delays to substitute frequency control.

Eq. 14 in the article can be rewritten as:

$$[S_{PE}]^{\omega_1,\omega_2,\omega_3,\omega_4}_{\boldsymbol{e}_1,\boldsymbol{e}_2,\boldsymbol{e}_3,\boldsymbol{e}_4}(\tau,T,t) \propto \sum_{p,q,r,s} C^p_{\omega_1} C^q_{\omega_2} C^r_{\omega_3} C^s_{\omega_4} \mathcal{G}_{gp}(\tau)\mathcal{G}_{sg}(t) P^{p,q,r,s}_{\boldsymbol{e}_1,\boldsymbol{e}_2,\boldsymbol{e}_3,\boldsymbol{e}_4}(0,T,0), \tag{S32}$$

For simplicity, we have made the approximations: $\mathcal{G}_{f\alpha}(t) \approx \mathcal{G}_{\beta g}(t)$ and $\mathcal{G}_{f\beta}(t) \approx \mathcal{G}_{\alpha g}(t)$. Notice that in Eq. S32, the frequency ω_{pg} appears both in the coherence time propagator $\mathcal{G}_{gp}(\tau)$ as well as in the frequency amplitude of the first transition $C^p_{\omega_1}$. A similar observation follows for ω_{sg} in the echo time in $\mathcal{G}_{sg}(t)$ and $C^s_{\omega_4}$. The frequency redundancy in the propagators and the transition amplitudes is the key to understand trading of frequency control for time delays.

Upon the collection of the signal along many values of τ and t for a fixed T, a double one-sided Fourier transformation yields the 2D-ES [4]:

$$S(\omega_\tau,T,\omega_t) = \int_0^\infty d\tau e^{-i\omega_\tau \tau} \int_0^\infty dt e^{i\omega_t t} [S_{PE}]^{\omega_1,\omega_2,\omega_3,\omega_4}_{\boldsymbol{e}_1,\boldsymbol{e}_2,\boldsymbol{e}_3,\boldsymbol{e}_4}(\tau,T,t) \tag{S33}$$

$$\propto \sum_{p,s=\alpha,\beta} l_{\tau,p}(\omega_\tau) l_{t,s}(\omega_t) S_{ps}(T) \tag{S34}$$

The spectrum consists of a sum of four resonances at $(\omega_\tau,\omega_t) \in \{(\omega_{\alpha g},\omega_{\alpha g}),(\omega_{\alpha g},\omega_{\beta g}),(\omega_{\beta g},\omega_{\alpha g}),(\omega_{\beta g},\omega_{\beta g})\}$, which correspond to the frequencies of the optical coherences at the coherence and echo times. These resonances are modulated by lineshape functions of the form,

$$l_{\tau,p}(\omega_\tau) = \frac{1}{i(\omega_\tau - \omega_{pg} - i\Gamma_{pg})}, \tag{S35}$$

$$l_{t,s}(\omega_t) = \frac{1}{i(-\omega_t + \omega_{sg} - i\Gamma_{sg})}, \tag{S36}$$

and the amplitude of each peak is given by

$$S_{ps}(T) = \sum_{q,r} C^p_{\omega_1} C^q_{\omega_2} C^r_{\omega_3} C^s_{\omega_4} P^{p,q,r,s}_{\boldsymbol{e}_1,\boldsymbol{e}_2,\boldsymbol{e}_3,\boldsymbol{e}_4}(0,T,0) \tag{S37}$$

In our original example for QPT, we considered sixteen possible four-pulse-combination experiments, which can isolate each of the $P^{p,q,r,s}_{\boldsymbol{e}_1,\boldsymbol{e}_2,\boldsymbol{e}_3,\boldsymbol{e}_4}(\tau,T,t)$ terms for $p,q,r,s \in \{\alpha,\beta\}$ for a fixed polarization setting $(\boldsymbol{e}_1,\boldsymbol{e}_2,\boldsymbol{e}_3,\boldsymbol{e}_4)$, which in turn yield enough information to invert the elements of $\chi(T)$. The pulses were assumed to be chosen from the toolbox in Eq. 13 in the article. The same sixteen experiments can be extended to the 2D-ES domain by collecting data from many τ and t values, so that $P^{p,q,r,s}_{\boldsymbol{e}_1,\boldsymbol{e}_2,\boldsymbol{e}_3,\boldsymbol{e}_4}(0,T,0) \propto P^{p,q,r,s}_{\boldsymbol{e}_1,\boldsymbol{e}_2,\boldsymbol{e}_3,\boldsymbol{e}_4}(\tau,T,t)$ can be extracted from Eq. S37, provided that the amplitudes $S_{ps}(T)$ can be obtained through a fitting procedure of the 2D-ES to a sum of the four lineshapes. However, we can get away with many fewer experiments. The amplitude $S_{ps}(T)$ only contains information of the Feynman diagrams where the first pulse is centered about ω_{pg} and the fourth pulse about ω_{sg}. Frequency control over the first and the fourth pulses is redundant, as it will yield 2D-spectra with only one peak at a time. This is unnecessary as each of the four peak amplitudes can be determined independently via a fitting procedure. Instead, a waveform that excites both $|\alpha\rangle$ and $|\beta\rangle$ with the same amplitude (e.g., a pulse with carrier frequency in between the excitons, $\bar{\omega} = \frac{\omega_\alpha+\omega_\beta}{2}$, and the same σ as before, or shorter) for these two perturbations will, in general, expose the four resonances in a single 2D-ES, so that $C^p_{\omega_1} = C^s_{\omega_4}$ for all p,s. However, selective waveforms, such as the ones described for the original QPT, must still be used for the second and third perturbations, as $S_{ps}(T)$ still contains a sum over q,r, which needs to be distilled.

The conclusion is that one can trade frequency control for time-delays for the first and fourth pulses, but not for the second and third pulses. For this trade to work, it is essential that no bath-induced coherence transfers occur during the coherence and echo times, so that we can write an optical propagator like Eq. 11 in the article.

X. SECULAR REDFIELD MODEL FOR MARKOVIAN DISSIPATION

The free evolution of the system S and bath B is generated by the total Hamiltonian

$$H_{\text{total}} = H_S + H_B + H_{SB} \tag{S38}$$

where H_S, H_B, and H_{SB} are the Hamiltonian for S, B, and the interaction between S and B, respectively. We model the bath as being constituted by two independent and identically

distributed Ohmic bosonic baths, each linearly coupled to a site of the dimer.

$$\begin{aligned} H_B &= \sum_{i=\alpha,\beta} \sum_x \omega_{x,i} \left(b_{x,i}^+ b_{x,i} + \frac{1}{2} \right) \\ H_{SB} &= F_\alpha |\alpha\rangle\langle\alpha| + F_\beta |\beta\rangle\langle\beta| + (F_\alpha + F_\beta)|f\rangle\langle f| \\ F_i &= \sum_x \lambda_{x,i} (b_{x,i} + b_{x,i}^+) \end{aligned} \tag{S39}$$

where $b_{x,i}$, $b_{x,i}^+$ are the anhilation and creation operators of the bath mode x coupled to the site i with frequency $\omega_{x,i}$, $\lambda_{x,i}$ is a coupling strength, and the spectral density is the same for both sites:

$$\begin{aligned} J_i(\omega) &= \sum_x \omega_{x,i}^2 \lambda_{x,i}^2 \delta(\omega - \omega_x) \\ &= \frac{\lambda}{\omega_c} \omega e^{-\omega/\omega_c}. \end{aligned} \tag{S40}$$

We take $\omega_c = 120$ cm^{-1} and $\lambda = 30$ cm^{-1}, which are typical energy scales for biomolecular chromophores. By applying second-order perturbation theory on H_{SB}, tracing over the degrees of freedom of B, and invoking the Markov and secular approximations, one can arrive at the Redfield equation [17],

$$\dot{\rho}(T) = -i[H_S, \rho(T)] - \mathcal{R}\rho(T), \tag{S41}$$

The Redfield tensor $\mathcal{R}$ [18] for $\underline{\mathrm{T}} = 273$ K is shown in Table S1. Table S2 shows the explicit expressions of $\chi(T)$ in terms of $\mathcal{R}$.

TABLE S1. Values (in ps^{-1}) of non-zero rates of the (secular) Redfield tensor at $\underline{\mathrm{T}} = 273$ K

$R_{\beta\beta\alpha\alpha}$	2.15
$R_{\alpha\alpha\beta\beta} = e^{-\omega_{\alpha\beta}/k_B \underline{\mathrm{T}}} R_{\beta\beta\alpha\alpha}$	0.467
$R_{\alpha\beta\alpha\beta} = R_{\beta\alpha\beta\alpha}$	6.91
$R_{\alpha g\alpha g} = R_{g\alpha g\alpha} = R_{f\alpha f\alpha} = R_{\alpha f\alpha f}$	6.95
$R_{\beta g\beta g} = R_{g\beta g\beta} = R_{f\beta f\beta} = R_{\beta f\beta f}$	6.11
$R_{fgfg} = R_{gfgf}$	17.9

TABLE S2. Analytical expressions for the nonzero elements of $\chi(T)$ involving single-exciton states

$\chi_{\alpha\alpha\alpha\alpha}(T)$	$e^{-R_{\beta\beta\alpha\alpha}T}$
$\chi_{\beta\beta\alpha\alpha}(T)$	$1 - e^{-R_{\beta\beta\alpha\alpha}T}$
$\chi_{\beta\beta\beta\beta}(T)$	$e^{-R_{\alpha\alpha\beta\beta}T}$
$\chi_{\alpha\alpha\beta\beta}(T)$	$1 - e^{-R_{\alpha\alpha\beta\beta}T}$
$\chi_{\alpha\beta\alpha\beta}(T) = (\chi_{\beta\alpha\beta\alpha}(T))^*$	$e^{-i\omega_{\alpha\beta}T} e^{-R_{\alpha\beta\alpha\beta}T}$

XI. RECONSTRUCTION OF $\chi(T)$

We divide the numerical reconstruction of $\chi(T)$ into two steps.

A. Reconstruction of the values $\langle P^{p,q,r,s}_{z,z,z,z}(\tau,T,t)\rangle_{iso}$ from the signals $\langle [S_{PE}]^{\omega_1,\omega_2,\omega_3,\omega_4}_{z,z,z,z}(\tau,T,t)\rangle_{iso}$

Eq. (14) in the article can be arranged into a matrix equation,

$$S_{PE}(\tau,T,t) \propto \mathbb{C}P(\tau,T,t) \tag{S42}$$

where S_{PE} is a vector of the sixteen measured signals $\langle [S_{PE}]^{\omega_1,\omega_2,\omega_3,\omega_4}_{z,,\boldsymbol{e}_3,\boldsymbol{e}_4}(\tau,T,t)\rangle_{iso}$, $P(\tau,T,t)$ is the vector consisting of the sixteen values $\langle P^{p,q,r,s}_{\boldsymbol{e}_1,\boldsymbol{e}_2,\boldsymbol{e}_3,\boldsymbol{e}_4}(\tau,T,t)\rangle_{iso}$ which are to be extracted, and $\mathbb{C}$ is a matrix of known pulse related coefficients $C^p_{\omega_1}C^q_{\omega_2}C^r_{\omega_3}C^s_{\omega_4}$. An important issue to address is the stability of the inversion of $P(\tau,T,t)$ subject to errors in $S_{PE}(\tau,T,t)$ upon changes in the ratio C_2/C_1 (see Eq. 13 in the article). Denote the spectral norm of a vector or a matrix with $\|\cdot\|$. We can bound the errors in the numerically extracted P from Eq. S42 in terms of the errors in the signal S_{PE} [19],

$$\frac{||\Delta P||}{||P||} \leq \kappa_{\mathbb{C}} \frac{\| \Delta S_{PE} \|}{\| S_{PE} \|}, \tag{S43}$$

where ΔP and ΔS_{PE} are errors in P and S_{PE}, respectively. The *condition number* $\kappa_{\mathbb{C}}$ is given by

$$\kappa_{\mathbb{C}} = \| \mathbb{C}(T) \| \| [\mathbb{C}(T)]^{-1} \|, \tag{S44}$$

yields a measure of the amplification of the relative errors on the inverted vector due to the relative errors in the experimental data. The lowest possible value for a condition number is 1. When both waveforms of the toolbox excite $|\alpha\rangle$ and $|\beta\rangle$ with the same amplitude ($C'/C" = 1$), there is no selectivity in the preparation and detection of states in the energy domain, and $\kappa_{\mathbb{C}} = \infty$, yielding the worst scenario for reconstruction. The best scenario occurs for the MDC case ($C'/C" \to \infty$), where $\mathbb{C}$ is proportional to the identity matrix, and $\kappa_{\mathbb{C}} = 1$.

Not surprisingly, $\kappa_{\mathbb{C}}$ decreases monotonically over the $C'/C" \in [1,\infty]$ range. Fig. S1 shows $\kappa_{\mathbb{C}}$ with respect to $C'/C"$. The small values of $\kappa_{\mathbb{C}}$ imply a robust numerical extraction of $P(\tau,T,t)$ over a wide range of obtainable $C'/C"$.

B. Reconstruction of $\chi(T)$ from $\langle P^{p,q,r,s}_{z,z,z,z}(\tau,T,t)\rangle_{iso}$

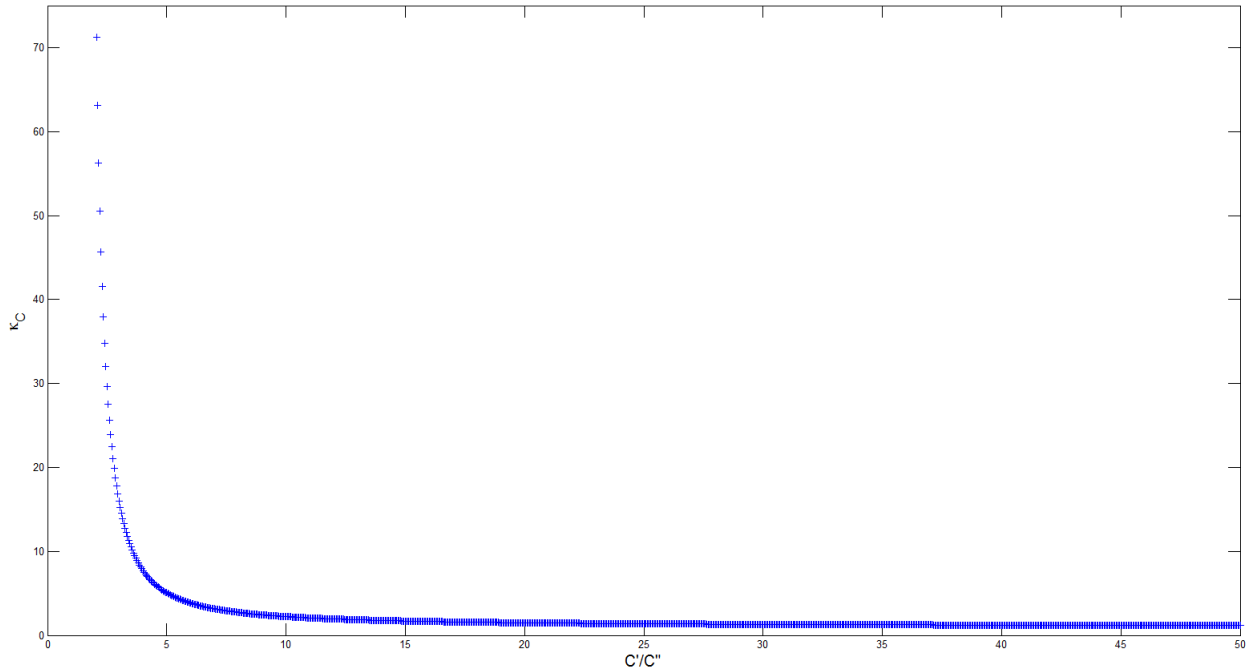

Figure S2: *Plot of* $\kappa_{\mathbb{C}}$ *vs.* C/C". The function decreases monotonically over $C'/C" \in [1, \infty]$, as expected, with $C'/C" = 1$ being the worst scenario of reconstruction corresponding to the case of equal pulse amplitude at both excitonic energies $\omega_{\alpha g}$ and $\omega_{\beta g}$, and $C'/C" = \infty$ being the best scenario corresponding to the MDC.

Table S3. A set of experiments which yields $\chi(T)$

From the data	we can reconstruct the elements	which explicitly listed are
$\left\{\begin{array}{c}\langle P^{\alpha,\alpha,\alpha,\alpha}_{z,z,z,z}(\tau,T,t)\rangle_{iso},\\ \langle P^{\alpha,\alpha,\alpha,\beta}_{z,z,z,z}(\tau,T,t)\rangle_{iso},\\ \langle P^{\alpha,\alpha,\beta.,\beta}_{z,z,z,z}(\tau,T,t)\rangle_{iso},\\ \langle P^{\alpha,\alpha,\beta,\alpha}_{z,z,z,z}(\tau,T,t)\rangle_{iso}\end{array}\right\}$	$\{\chi_{ij\alpha\alpha}(T)\}$	$\left\{\begin{array}{c}\chi_{\alpha\alpha\alpha\alpha}(T),\\ \chi_{\beta\beta\alpha\alpha}(T),\\ \Re\{\chi_{\alpha\beta\alpha\alpha}(T)\}=\Re\{\chi_{\beta\alpha\alpha\alpha}(T)\},\\ \Im\{\chi_{\alpha\beta\alpha\alpha}(T)\}=-\Im\{\chi_{\beta\alpha\alpha\alpha}(T)\}\end{array}\right\}$
$\left\{\begin{array}{c}\langle P^{\beta,\beta,\alpha,\alpha}_{z,z,z,z}(\tau,T,t)\rangle_{iso},\\ \langle P^{\beta,\beta,\alpha,\beta}_{z,z,z,z}(\tau,T,t)\rangle_{iso},\\ \langle P^{\beta,\beta,\beta\beta}_{z,z,z,z}(\tau,T,t)\rangle_{iso},\\ \langle P^{\beta,\beta,\alpha,\beta}_{z,z,z,z}(\tau,T,t)\rangle_{iso}\end{array}\right\}$	$\{\chi_{ij\beta\beta}(T)\}$	$\left\{\begin{array}{c}\chi_{\alpha\alpha\beta\beta}(T),\\ \chi_{\beta\beta\beta\beta}(T),\\ \Re\{\chi_{\alpha\beta\beta\beta}(T)\}=\Re\{\chi_{\beta\alpha\beta\beta}(T)\},\\ \Im\{\chi_{\alpha\beta\beta\beta}(T)\}=-\Im\{\chi_{\beta\alpha\beta\beta}(T)\}\end{array}\right\}$
$\left\{\begin{array}{c}\langle P^{\beta,\alpha,\alpha,\alpha}_{z,z,z,z}(\tau,T,t)\rangle_{iso},\\ \langle P^{\beta,\alpha,\alpha,\beta}_{z,z,z,z}(\tau,T,t)\rangle_{iso},\\ \langle P^{\beta,\alpha,\beta,\beta}_{z,x,x,z}(\tau,T,t)\rangle_{iso},\\ \langle P^{\beta,\alpha,\beta,\alpha}_{z,x,x,z}(\tau,T,t)\rangle_{iso},\\ \langle P^{\alpha,\beta,\alpha,\alpha}_{z,z,z,z}(\tau,T,t)\rangle_{iso},\\ \langle P^{\alpha,\beta,\alpha,\beta}_{z,z,z,z}(\tau,T,t)\rangle_{iso},\\ \langle P^{\alpha,\beta,\beta,\beta}_{z,z,z,z}(\tau,T,t)\rangle_{iso},\\ \langle P^{\alpha,\beta,\beta,\alpha}_{z,z,z,z}(\tau,T,t)\rangle_{iso}\end{array}\right\}$	$\{\chi_{ij\alpha\beta}(T)=(\chi_{ji\beta\alpha}(T))^*\}$	$\left\{\begin{array}{rcl}\Re\{\chi_{\alpha\alpha\alpha\beta}(T)\} &=& \Re\{\chi_{\alpha\alpha\beta\alpha}(T)\},\\ \Im\{\chi_{\alpha\alpha\alpha\beta}(T)\} &=& -\Im\{\chi_{\alpha\alpha\beta\alpha}(T)\},\\ \Re\{\chi_{\beta\beta\alpha\beta}(T)\} &=& \Re\{\chi_{\beta\beta\beta\alpha}(T)\},\\ \Im\{\chi_{\beta\beta\alpha\beta}(T)\} &=& -\Im\{\chi_{\beta\beta\beta\alpha}(T)\},\\ \Re\{\chi_{\alpha\beta\alpha\beta}(T)\} &=& \Re\{\chi_{\beta\alpha\beta\alpha}(T)\},\\ \Im\{\chi_{\alpha\beta\alpha\beta}(T)\} &=& -\Im\{\chi_{\beta\alpha\beta\alpha}(T)\},\\ \Re\{\chi_{\beta\alpha\alpha\beta}(T)\} &=& \Re\{\chi_{\alpha\beta\beta\alpha}(T)\},\\ \Im\{\chi_{\alpha\beta\alpha\beta}(T)\} &=& -\Im\{\chi_{\beta\alpha\beta\alpha}(T)\}\end{array}\right\}$

Once the $\langle P^{p,q,r,s}_{z,z,z,z}(\tau,T,t)\rangle_{iso}$ values have been extracted, a second step to extract $\chi(T)$ from them is required. The explicit trace preservation identities,

$$\begin{aligned}
\chi_{gg\alpha\alpha}(T)-1 &= -\chi_{\alpha\alpha\alpha\alpha}(T)-\chi_{\beta\beta\alpha\alpha}(T)),\\
\chi_{gg\beta\beta}(T)-1 &= -\chi_{\alpha\alpha\beta\beta}(T)-\chi_{\beta\beta\beta\beta}(T)),\\
\Re\{\chi_{gg\alpha\beta}(T)\} &= -\Re\{\chi_{\alpha\alpha\alpha\beta}(T)\}-\Re\{\chi_{\beta\beta\alpha\beta}(T)\},\\
\Im\{\chi_{gg\alpha\beta}(T)\} &= -\Im\{\chi_{\alpha\alpha\alpha\beta}(T)\}-\Im\{\chi_{\beta\beta\alpha\beta}(T)\},
\end{aligned} \tag{S45}$$

together with the Hermiticity identities in column 2 of Table S3, can be substituted into Eqs. 14-16 in the article, and their analogues upon the $\alpha \leftrightarrow \beta$ substitution. After isotropic averaging, we can write the matrix equations,

$$\mathbb{M}^{qp}X^{qp}(T)=P^{qp}(T), \tag{S46}$$

each of them corresponding to an initial state qp. The analytical expressions of the square matrices $\mathbb{M}^{qp}$ are listed in Tables S4, S5, and S6. The real vectors X to extract contain the

elements of the process matrix,

$$
\begin{aligned}
X^{\alpha\alpha}(T) &= \begin{bmatrix} \chi_{\alpha\alpha\alpha\alpha}(T) \\ \chi_{\beta\beta\alpha\alpha}(T) \\ \Re\{\chi_{\alpha\beta\alpha\alpha}(T)\} \\ \Im\{\chi_{\alpha\beta\alpha\alpha}(T)\} \end{bmatrix}, \\
X^{\beta\beta}(T) &= \begin{bmatrix} \chi_{\alpha\alpha\beta\beta}(T) \\ \chi_{\beta\beta\beta\beta}(T) \\ \Re\{\chi_{\alpha\beta\beta\beta}(T)\} \\ \Im\{\chi_{\alpha\beta\beta\beta}(T)\} \end{bmatrix}, \\
X^{\alpha\beta}(T) &= \begin{bmatrix} \Re\{\chi_{\alpha\alpha\alpha\beta}(T)\} \\ \Re\{\chi_{\beta\beta\alpha\beta}(T)\} \\ \Re\{\chi_{\alpha\beta\alpha\beta}(T)\} \\ \Re\{\chi_{\beta\alpha\alpha\beta}(T)\} \\ \Im\{\chi_{\alpha\alpha\alpha\beta}(T)\} \\ \Im\{\chi_{\beta\beta\alpha\beta}(T)\} \\ \Im\{\chi_{\alpha\beta\alpha\beta}(T)\} \\ \Im\{\chi_{\beta\alpha\alpha\beta}(T)\} \end{bmatrix},
\end{aligned}
\tag{S47}
$$

whereas the vectors consisting of data from experiments are

$$
\begin{aligned}
P^{\alpha\alpha}(T) &= \begin{bmatrix} \langle P^{\alpha,\alpha,\alpha,\alpha}_{z,z,z,z}(0,T,0)\rangle_{iso} \\ \langle P^{\alpha,\alpha,\alpha,\beta}_{z,z,z,z}(0,T,0)\rangle_{iso} \\ \langle P^{\alpha,\alpha,\beta,\alpha}_{z,z,z,z}(0,T,0)\rangle_{iso} \\ \langle P^{\alpha,\alpha,\beta,\beta}_{z,z,z,z}(0,T,0)\rangle_{iso} \end{bmatrix}, \\
P^{\beta\beta}(T) &= \begin{bmatrix} \langle P^{\beta,\beta,\alpha,\alpha}_{z,z,z,z}(0,T,0)\rangle_{iso} \\ \langle P^{\beta,\beta,\alpha,\beta}_{z,z,z,z}(0,T,0)\rangle_{iso} \\ \langle P^{\beta,\beta,\beta,\alpha}_{z,z,z,z}(0,T,0)\rangle_{iso} \\ \langle P^{\beta,\beta,\beta,\beta}_{z,z,z,z}(0,T,0)\rangle_{iso} \end{bmatrix}, \\
P^{\alpha\beta}(T) &= \begin{bmatrix} \langle P^{\beta,\alpha,\alpha,\alpha}_{z,z,z,z}(0,T,0)\rangle_{iso} \\ \langle P^{\beta,\alpha,\alpha,\beta}_{z,z,z,z}(0,T,0)\rangle_{iso} \\ \langle P^{\beta,\alpha,\beta,\alpha}_{z,z,z,z}(0,T,0)\rangle_{iso} \\ \langle P^{\beta,\alpha,\beta,\beta}_{z,z,z,z}(0,T,0)\rangle_{iso} \\ \langle P^{\alpha,\beta,\alpha,\alpha}_{z,z,z,z}(0,T,0)\rangle_{iso} \\ \langle P^{\alpha,\beta,\alpha,\beta}_{z,z,z,z}(0,T,0)\rangle_{iso} \\ \langle P^{\alpha,\beta,\beta,\alpha}_{z,z,z,z}(0,T,0)\rangle_{iso} \\ \langle P^{\alpha,\beta,\beta,\beta}_{z,z,z,z}(0,T,0)\rangle_{iso} \end{bmatrix}.
\end{aligned}
$$

Construction of the $P^{qp}(T)$ vectors can be done from the values $\langle P^{p,q,r,s}_{z,z,z,z}(0,T,0)\rangle_{iso}$ stemming from TD/TB measurements, or alternatively, after factoring the coherence and echo propagators from the values $\langle P^{p,q,r,s}_{z,z,z,z}(\tau,T,t)\rangle_{iso}$ given by the general rephasing PE experiment, as in Eq. S32.

Table S4. Entries of $\mathbb{M}^{\alpha\alpha}$

ROW	*COLUMN*	*VALUE*
1	1	$\frac{2\mu_{\alpha g}^4}{5}$
1	2	$\frac{\mu_{\alpha g}^4}{5} - \frac{1}{15}\left(\cos\left(2\theta_{f\beta}\right)+2\right)\mu_{f\beta}^2\mu_{\alpha g}^2$
1	3	0
1	4	0
2	1	0
2	2	0
2	3	$\frac{1}{15}\mu_{\alpha g}^2\left(3\cos\left(\theta_{\beta g}\right)\mu_{\alpha g}\mu_{\beta g} - \left(3\cos\left(\theta_{f\alpha}\right)\cos\left(\theta_{f\beta}\right)+\sin\left(\theta_{f\alpha}\right)\sin\left(\theta_{f\beta}\right)\right)\mu_{f\alpha}\mu_{f\beta}\right)$
2	4	$\frac{1}{15}i\mu_{\alpha g}^2\left(\left(3\cos\left(\theta_{f\alpha}\right)\cos\left(\theta_{f\beta}\right)+\sin\left(\theta_{f\alpha}\right)\sin\left(\theta_{f\beta}\right)\right)\mu_{f\alpha}\mu_{f\beta} - 3\cos\left(\theta_{\beta g}\right)\mu_{\alpha g}\mu_{\beta g}\right)$
3	1	0
3	2	0
3	3	$\frac{1}{15}\mu_{\alpha g}^2\left(3\cos\left(\theta_{\beta g}\right)\mu_{\alpha g}\mu_{\beta g} - \left(3\cos\left(\theta_{f\alpha}\right)\cos\left(\theta_{f\beta}\right)+\sin\left(\theta_{f\alpha}\right)\sin\left(\theta_{f\beta}\right)\right)\mu_{f\alpha}\mu_{f\beta}\right)$
3	4	$-\frac{1}{15}i\mu_{\alpha g}^2\left(\left(3\cos\left(\theta_{f\alpha}\right)\cos\left(\theta_{f\beta}\right)+\sin\left(\theta_{f\alpha}\right)\sin\left(\theta_{f\beta}\right)\right)\mu_{f\alpha}\mu_{f\beta} - 3\cos\left(\theta_{\beta g}\right)\mu_{\alpha g}\mu_{\beta g}\right)$
4	1	$\frac{1}{15}\mu_{\alpha g}^2\left(\left(\cos\left(2\theta_{\beta g}\right)+2\right)\mu_{\beta g}^2 - \left(\cos\left(2\theta_{f\alpha}\right)+2\right)\mu_{f\alpha}^2\right)$
4	2	$\frac{2}{15}\left(\cos\left(2\theta_{\beta g}\right)+2\right)\mu_{\alpha g}^2\mu_{\beta g}^2$
4	3	0
4	4	0

Table S5. Entries of $\mathbb{M}^{\beta\beta}$

ROW	*COLUMN*	*VALUE*
1	1	$\frac{2}{15}\left(\cos\left(2\theta_{\beta g}\right)+2\right)\mu_{\alpha g}^2\mu_{\beta g}^2$
1	2	$\frac{1}{15}\left(\left(\cos\left(2\theta_{\beta g}\right)+2\right)\mu_{\alpha g}^2 - \left(\cos\left(2\left(\theta_{f\beta}-\theta_{\beta g}\right)\right)+2\right)\mu_{f\beta}^2\right)\mu_{\beta g}^2$
1	3	0
1	4	0
2	1	0
2	2	0
2	3	$\frac{1}{15}\mu_{\beta g}^2\left(3\cos\left(\theta_{\beta g}\right)\mu_{\alpha g}\mu_{\beta g} - \left(2\cos\left(\theta_{f\alpha}-\theta_{f\beta}\right)+\cos\left(\theta_{f\alpha}+\theta_{f\beta}-2\theta_{\beta g}\right)\right)\mu_{f\alpha}\mu_{f\beta}\right)$
2	4	$\frac{1}{15}i\mu_{\beta g}^2\left(\left(2\cos\left(\theta_{f\alpha}-\theta_{f\beta}\right)+\cos\left(\theta_{f\alpha}+\theta_{f\beta}-2\theta_{\beta g}\right)\right)\mu_{f\alpha}\mu_{f\beta} - 3\cos\left(\theta_{\beta g}\right)\mu_{\alpha g}\mu_{\beta g}\right)$
3	1	0
3	2	0
3	3	$\frac{1}{15}\mu_{\beta g}^2\left(3\cos\left(\theta_{\beta g}\right)\mu_{\alpha g}\mu_{\beta g} - \left(2\cos\left(\theta_{f\alpha}-\theta_{f\beta}\right)+\cos\left(\theta_{f\alpha}+\theta_{f\beta}-2\theta_{\beta g}\right)\right)\mu_{f\alpha}\mu_{f\beta}\right)$
3	4	$\frac{1}{15}i\mu_{\beta g}^2\left(3\cos\left(\theta_{\beta g}\right)\mu_{\alpha g}\mu_{\beta g} - \left(2\cos\left(\theta_{f\alpha}-\theta_{f\beta}\right)+\cos\left(\theta_{f\alpha}+\theta_{f\beta}-2\theta_{\beta g}\right)\right)\mu_{f\alpha}\mu_{f\beta}\right)$
4	1	$\frac{1}{15}\mu_{\beta g}^2\left(3\mu_{\beta g}^2 - \left(\cos\left(2\left(\theta_{f\alpha}-\theta_{\beta g}\right)\right)+2\right)\mu_{f\alpha}^2\right)$
4	2	$\frac{2\mu_{\beta g}^4}{5}$
4	3	0
4	4	0

Table S6. Entries of $\mathbb{M}^{\alpha\beta}$

ROW	*COLUMN*	*VALUE*
1	1	$\frac{2}{5}\cos\left(\theta_{\beta\mathrm{g}}\right)\mu_{\alpha\mathrm{g}}^{3}\mu_{\beta\mathrm{g}}$
1	2	$\frac{1}{15}\mu_{\alpha\mathrm{g}}\left(3\cos\left(\theta_{\beta\mathrm{g}}\right)\mu_{\alpha\mathrm{g}}^{2}-\left(\cos\left(2\theta_{\mathrm{f}\beta}-\theta_{\beta\mathrm{g}}\right)+2\cos\left(\theta_{\beta\mathrm{g}}\right)\right)\mu_{\mathrm{f}\beta}^{2}\right)\mu_{\beta\mathrm{g}}$
1	3	0
1	4	0
1	5	$\frac{2}{5}i\cos\left(\theta_{\beta\mathrm{g}}\right)\mu_{\alpha\mathrm{g}}^{3}\mu_{\beta\mathrm{g}}$
1	6	$-\frac{1}{15}i\mu_{\alpha\mathrm{g}}\left(\left(\cos\left(2\theta_{\mathrm{f}\beta}-\theta_{\beta\mathrm{g}}\right)+2\cos\left(\theta_{\beta\mathrm{g}}\right)\right)\mu_{\mathrm{f}\beta}^{2}-3\cos\left(\theta_{\beta\mathrm{g}}\right)\mu_{\alpha\mathrm{g}}^{2}\right)\mu_{\beta\mathrm{g}}$
1	7	0
1	8	0
2	1	0
2	2	0
2	3	0
2	4	$\frac{1}{15}\mu_{\alpha\mathrm{g}}\mu_{\beta\mathrm{g}}\left(\left(\cos\left(2\theta_{\beta\mathrm{g}}\right)+2\right)\mu_{\alpha\mathrm{g}}\mu_{\beta\mathrm{g}}-\left(\cos\left(\theta_{\mathrm{f}\alpha}-\theta_{\mathrm{f}\beta}-\theta_{\beta\mathrm{g}}\right)+2\cos\left(\theta_{\mathrm{f}\alpha}\right)\cos\left(\theta_{\mathrm{f}\beta}-\theta_{\beta\mathrm{g}}\right)\right)\mu_{\mathrm{f}\alpha}\mu_{\mathrm{f}\beta}\right)$
2	5	0
2	6	0
2	7	0
2	8	$\frac{1}{15}i\mu_{\alpha\mathrm{g}}\mu_{\beta\mathrm{g}}\left(\left(\cos\left(2\theta_{\beta\mathrm{g}}\right)+2\right)\mu_{\alpha\mathrm{g}}\mu_{\beta\mathrm{g}}-\left(\cos\left(\theta_{\mathrm{f}\alpha}-\theta_{\mathrm{f}\beta}-\theta_{\beta\mathrm{g}}\right)+2\cos\left(\theta_{\mathrm{f}\alpha}\right)\cos\left(\theta_{\mathrm{f}\beta}-\theta_{\beta\mathrm{g}}\right)\right)\mu_{\mathrm{f}\alpha}\mu_{\mathrm{f}\beta}\right)$
3	1	0
3	2	0
3	3	$\frac{1}{15}\mu_{\alpha\mathrm{g}}\mu_{\beta\mathrm{g}}\left(\left(\cos\left(2\theta_{\beta\mathrm{g}}\right)+2\right)\mu_{\alpha\mathrm{g}}\mu_{\beta\mathrm{g}}-\left(\cos\left(\theta_{\mathrm{f}\alpha}-\theta_{\mathrm{f}\beta}-\theta_{\beta\mathrm{g}}\right)+2\cos\left(\theta_{\mathrm{f}\alpha}\right)\cos\left(\theta_{\mathrm{f}\beta}-\theta_{\beta\mathrm{g}}\right)\right)\mu_{\mathrm{f}\alpha}\mu_{\mathrm{f}\beta}\right)$
3	4	0
3	5	0
3	6	0
3	7	$\frac{1}{15}i\mu_{\alpha\mathrm{g}}\mu_{\beta\mathrm{g}}\left(\left(\cos\left(2\theta_{\beta\mathrm{g}}\right)+2\right)\mu_{\alpha\mathrm{g}}\mu_{\beta\mathrm{g}}-\left(\cos\left(\theta_{\mathrm{f}\alpha}-\theta_{\mathrm{f}\beta}-\theta_{\beta\mathrm{g}}\right)+2\cos\left(\theta_{\mathrm{f}\alpha}\right)\cos\left(\theta_{\mathrm{f}\beta}-\theta_{\beta\mathrm{g}}\right)\right)\mu_{\mathrm{f}\alpha}\mu_{\mathrm{f}\beta}\right)$
3	8	0
4	1	$\frac{1}{15}\mu_{\alpha\mathrm{g}}\mu_{\beta\mathrm{g}}\left(3\cos\left(\theta_{\beta\mathrm{g}}\right)\mu_{\beta\mathrm{g}}^{2}-\left(\cos\left(2\theta_{\mathrm{f}\alpha}-\theta_{\beta\mathrm{g}}\right)+2\cos\left(\theta_{\beta\mathrm{g}}\right)\right)\mu_{\mathrm{f}\alpha}^{2}\right)$
4	2	$\frac{2}{5}\cos\left(\theta_{\beta\mathrm{g}}\right)\mu_{\alpha\mathrm{g}}\mu_{\beta\mathrm{g}}^{3}$
4	3	0
4	4	0
4	5	$-\frac{1}{15}i\mu_{\alpha\mathrm{g}}\mu_{\beta\mathrm{g}}\left(\left(\cos\left(2\theta_{\mathrm{f}\alpha}-\theta_{\beta\mathrm{g}}\right)+2\cos\left(\theta_{\beta\mathrm{g}}\right)\right)\mu_{\mathrm{f}\alpha}^{2}-3\cos\left(\theta_{\beta\mathrm{g}}\right)\mu_{\beta\mathrm{g}}^{2}\right)$
4	6	$\frac{2}{5}i\cos\left(\theta_{\beta\mathrm{g}}\right)\mu_{\alpha\mathrm{g}}\mu_{\beta\mathrm{g}}^{3}$
4	7	0
4	8	0

Table S6 (continued). Entries of $\mathbb{M}^{\alpha\beta}$

ROW	*COLUMN*	*VALUE*
5	1	$\frac{2}{5}\cos\left(\theta_{\beta g}\right)\mu_{\alpha g}^{3}\mu_{\beta g}$
5	2	$\frac{1}{15}\mu_{\alpha g}\left(3\cos\left(\theta_{\beta g}\right)\mu_{\alpha g}^{2}-\left(\cos\left(2\theta_{f\beta}-\theta_{\beta g}\right)+2\cos\left(\theta_{\beta g}\right)\right)\mu_{f\beta}^{2}\right)\mu_{\beta g}$
5	3	0
5	4	0
5	5	$-\frac{2}{5}i\cos\left(\theta_{\beta g}\right)\mu_{\alpha g}^{3}\mu_{\beta g}$
5	6	$\frac{1}{15}i\mu_{\alpha g}\left(\left(\cos\left(2\theta_{f\beta}-\theta_{\beta g}\right)+2\cos\left(\theta_{\beta g}\right)\right)\mu_{f\beta}^{2}-3\cos\left(\theta_{\beta g}\right)\mu_{\alpha g}^{2}\right)\mu_{\beta g}$
5	7	0
5	8	0
6	1	0
6	2	0
6	3	$\frac{1}{15}\mu_{\alpha g}\mu_{\beta g}\left(\left(\cos\left(2\theta_{\beta g}\right)+2\right)\mu_{\alpha g}\mu_{\beta g}-\left(\cos\left(\theta_{f\alpha}-\theta_{f\beta}-\theta_{\beta g}\right)+2\cos\left(\theta_{f\alpha}\right)\cos\left(\theta_{f\beta}-\theta_{\beta g}\right)\right)\mu_{f\alpha}\mu_{f\beta}\right)$
6	4	0
6	5	0
6	6	0
6	7	$\frac{1}{15}i\mu_{\alpha g}\mu_{\beta g}\left(\left(\cos\left(\theta_{f\alpha}-\theta_{f\beta}-\theta_{\beta g}\right)+2\cos\left(\theta_{f\alpha}\right)\cos\left(\theta_{f\beta}-\theta_{\beta g}\right)\right)\mu_{f\alpha}\mu_{f\beta}-\left(\cos\left(2\theta_{\beta g}\right)+2\right)\mu_{\alpha g}\mu_{\beta g}\right)$
6	8	0
7	1	0
7	2	0
7	3	0
7	4	$\frac{1}{15}\mu_{\alpha g}\mu_{\beta g}\left(\left(\cos\left(2\theta_{\beta g}\right)+2\right)\mu_{\alpha g}\mu_{\beta g}-\left(\cos\left(\theta_{f\alpha}-\theta_{f\beta}-\theta_{\beta g}\right)+2\cos\left(\theta_{f\alpha}\right)\cos\left(\theta_{f\beta}-\theta_{\beta g}\right)\right)\mu_{f\alpha}\mu_{f\beta}\right)$
7	5	0
7	6	0
7	7	0
7	8	$\frac{1}{15}i\mu_{\alpha g}\mu_{\beta g}\left(\left(\cos\left(\theta_{f\alpha}-\theta_{f\beta}-\theta_{\beta g}\right)+2\cos\left(\theta_{f\alpha}\right)\cos\left(\theta_{f\beta}-\theta_{\beta g}\right)\right)\mu_{f\alpha}\mu_{f\beta}-\left(\cos\left(2\theta_{\beta g}\right)+2\right)\mu_{\alpha g}\mu_{\beta g}\right)$
8	1	$\frac{1}{15}\mu_{\alpha g}\mu_{\beta g}\left(3\cos\left(\theta_{\beta g}\right)\mu_{\beta g}^{2}-\left(\cos\left(2\theta_{f\alpha}-\theta_{\beta g}\right)+2\cos\left(\theta_{\beta g}\right)\right)\mu_{f\alpha}^{2}\right)$
8	2	$\frac{2}{5}\cos\left(\theta_{\beta g}\right)\mu_{\alpha g}\mu_{\beta g}^{3}$
8	3	0
8	4	0
8	5	$\frac{1}{15}i\mu_{\alpha g}\mu_{\beta g}\left(\left(\cos\left(2\theta_{f\alpha}-\theta_{\beta g}\right)+2\cos\left(\theta_{\beta g}\right)\right)\mu_{f\alpha}^{2}-3\cos\left(\theta_{\beta g}\right)\mu_{\beta g}^{2}\right)$
8	6	$-\frac{2}{5}i\cos\left(\theta_{\beta g}\right)\mu_{\alpha g}\mu_{\beta g}^{3}$
8	7	0
8	8	0

The matrices $\mathbb{M}^{qp}$ can be easily reexpressed in terms of d_A, d_B, ϕ, and θ using the equations in section I. As in subsection A, we obtain a bound on the relative error of $X^{qp}(T)$ [19, 20]:

$$\frac{||\Delta X^{qp}(T)||}{||X^{qp}(T)||} \leq \kappa^{qp}\frac{\| \Delta P^{qp}(T) \|}{\| P^{qp}(T) \|}. \tag{S48}$$

The condition number κ^{qp} is given by,

$$\kappa^{qp} = \| \mathbb{M}^{qp} \| \| [\mathbb{M}^{qp}]^{-1} \| . \tag{S49}$$

Fig. S2 shows contour plots of $\kappa \equiv \max_{qp}\kappa$ for a set of fixed dipole norm ratios d_B/d_A across the entire range of angles $0 \leq \theta, \phi < \pi$. For $d_B/d_A = 1$ (panel (a)), there are four stripes for which the QPT protocol fails. The stripes along $\theta = 0, \frac{\pi}{2}$ correspond to the absence of excitonic coupling ($J = 0$), whereas the ones along $\theta = \frac{\pi}{4}, \frac{3\pi}{4}$ correspond to the homodimer

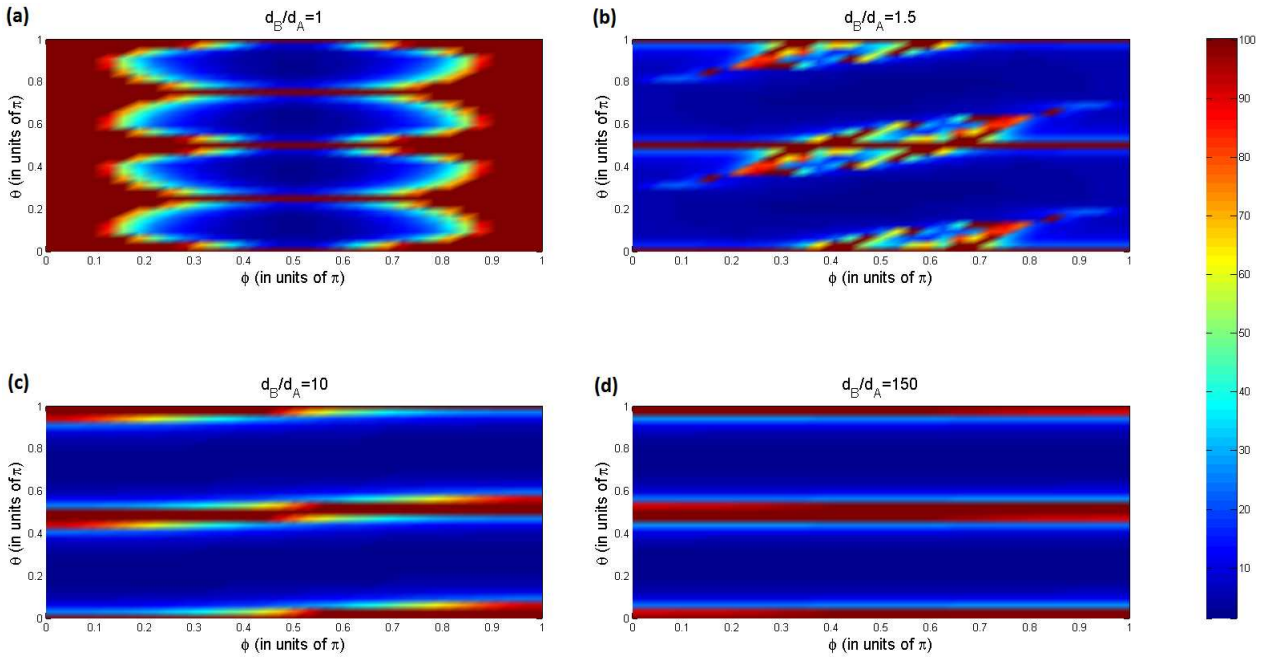

Figure S3: *Contour plots of* κ *vs.* θ and ϕ. The stripes about $\theta = 0, \frac{\pi}{2}$ correspond to the case of uncoupled chromophores, and fail to provide a QPT via our suggested protocol. Additional unstable regions emerge about $\theta = \frac{\pi}{4}, \frac{3\pi}{4}$ for $d_B/d_A = 1$ (panel (a)), which correspond to the homodimer case. The $\theta = \pi$ case is equivalent to the $\theta = 0$ case. Note that beyond the unstable regions, QPT is very robust, with condition number κ values on the order of 1 to 10.

case. As explained in Ref. [4], isotropic averages of signal denoting coherence to population or opposite processes vanish for a homodimer. Therefore, QPT is incomplete in those cases and large condition numbers arise near those critical angles. QPT is, however, quite robust in the wide range of structural parameters which do not lie in the critical stripes, with κ values on the order of 1 to 10. For $d_B/d_A = 1.5, 10, 100$ (panels (b), (c) and (d)), there is no possibility of homodimer, and in fact, the inversion only fails for the uncoupled chromophores situation. In general, the κ dependence on θ, ϕ is seen to be largely insensitive to the ratio $d_B/d_A \neq 1$. This phenomenon can be easily understood as follows: as long as there is coupling between the site excitons, the oscillator strength is fairly distributed between the two eigenstates of the single-exciton manifold even if their site oscillator strengths differ by many orders of magnitude.

Remarkably, the protocol does not fail for the $\phi = 0, \pi$ cases, when the site dipoles are aligned or antialigned, except when $d_B/d_A = 1$. For the latter, it happens that $\boldsymbol{\mu}_{\alpha g} = \boldsymbol{\mu}_{f\alpha}$ and $\boldsymbol{\mu}_{\beta g} = \boldsymbol{\mu}_{f\beta}$, yielding singular matrices $\mathbb{M}^{qp}$. For these particular ϕ values and general d_B/d_A ratios, the four parallel transition dipoles have different magnitude but the same direction. Since the currently proposed spectroscopic addressing of the states is through frequency space rather than through polarization, these degeneracies are unimportant.

C. Choosing sixteen measurements out of the thirty-two heterodyne detections

Table S3 explicitly lists all 16 elements of $\chi(T)$ which are extracted from the QPT protocol. As mentioned above, there are $2^4 - 2^2 = 12$ independent real-valued parameters associated to the dynamics in the single exciton manifold, but we also keep track of four leakage errors $\chi_{gg\alpha\alpha}(T)$, $\chi_{gg\beta\beta}(T)$, and $\Re\{\chi_{gg\alpha\beta}(T)\}$ and $\Im\{\chi_{gg\alpha\beta}(T)\}$, yielding a total of sixteen parameters to extract. The terms associated with these transfers to the ground state are not listed, as they can be expressed in terms of the rest of the elements using Eq. (3) in the article. The sixteen experiments described in the article involve thirty-two heterodyne real valued measurements, twice as many as parameters to extract. Clearly, there must be a way to select only sixteen measurements out of the thirty-two. We now show that this reduction is feasible and has similar stability properties as the original set. It is important to emphasize that the thirty-two or sixteen required heterodyne detections are one-dimensional (1D) measurements, as the signals $\langle [S_{PE}]^{\omega_1,\omega_2,\omega_3,\omega_4}_{\boldsymbol{e}_1,\boldsymbol{e}_2,\boldsymbol{e}_3,\boldsymbol{e}_4}(\tau,T,t)\rangle_{iso}$ stemming from a single pair of τ, t values suffice for the purposes of performing a QPT.

We first make some observations which are easily generalizable. Altogether, the four terms $\Re\{\langle P^{\alpha,\alpha,\alpha,\alpha}_{\boldsymbol{e}_1,\boldsymbol{e}_2,\boldsymbol{e}_3,\boldsymbol{e}_4}(\tau,T,t)\rangle_{iso}\}$, $\Im\{\langle P^{\alpha,\alpha,\alpha,\alpha}_{\boldsymbol{e}_1,\boldsymbol{e}_2,\boldsymbol{e}_3,\boldsymbol{e}_4}(\tau,T,t)\rangle_{iso}\}$, $\Re\{\langle P^{\alpha,\alpha,\beta,\beta}_{\boldsymbol{e}_1,\boldsymbol{e}_2,\boldsymbol{e}_3,\boldsymbol{e}_4}(\tau,T,t)\rangle_{iso}\}$, and $\Im\{\langle P^{\alpha,\alpha,\beta,\beta}_{\boldsymbol{e}_1,\boldsymbol{e}_2,\boldsymbol{e}_3,\boldsymbol{e}_4}(\tau,T,t)\rangle_{iso}\}$ contain information about the real valued population transfer terms $\chi_{\alpha\alpha\alpha\alpha}(T)$ and $\chi_{\beta\beta\alpha\alpha}(T)$. Consider the case where $\mathcal{G}_{gp}(\tau)\mathcal{G}_{ps}(t) \in \Re$ (for example, taking τ and t to satisfy $\omega_{gp}\tau = \omega_{ps}t = 2\pi$). Then, only $\Re\{\langle P^{\alpha,\alpha,\alpha,\alpha}_{\boldsymbol{e}_1,\boldsymbol{e}_2,\boldsymbol{e}_3,\boldsymbol{e}_4}(\tau,T,t)\rangle_{iso}\}$ and $\Re\{\langle P^{\alpha,\alpha,\beta,\beta}_{\boldsymbol{e}_1,\boldsymbol{e}_2,\boldsymbol{e}_3,\boldsymbol{e}_4}(\tau,T,t)\rangle_{iso}\}$ need to be monitored, as $\Im\{\langle P^{\alpha,\alpha,\alpha,\alpha}_{\boldsymbol{e}_1,\boldsymbol{e}_2,\boldsymbol{e}_3,\boldsymbol{e}_4}(\tau,T,t)\rangle_{iso}\}$ and $\Im\{\langle P^{\alpha,\alpha,\beta,\beta}_{\boldsymbol{e}_1,\boldsymbol{e}_2,\boldsymbol{e}_3,\boldsymbol{e}_4}(\tau,T,t)\rangle_{iso}\}$ will, in principle, vanish. Conversely, if $\mathcal{G}_{gp}(\tau)\mathcal{G}_{ps}(t) \in \Im$ (say, by taking $\omega_{gp}\tau = \frac{\pi}{2}$ and $\omega_{ps}t = 2\pi$), only the imaginary parts need to be monitored. Finally, if $\mathcal{G}_{gp}(\tau)\mathcal{G}_{ps}(t)$ has both real and complex parts of similar proportions, either the real or the imaginary parts suffice. Naturally, depending on the ratio between the magnitudes of the real and imaginary parts of $\mathcal{G}_{gp}(\tau)\mathcal{G}_{ps}(t)$, it will be numerically more favorable to measure the real or the imaginary parts of the signal.

Consider now the signals $\Re\{\langle P^{\beta,\alpha,\beta,\alpha}_{z,z,z,z}(\tau,T,t)\rangle_{iso}\}$, $\Im\{\langle P^{\beta,\alpha,\beta,\alpha}_{z,z,z,z}(\tau,T,t)\rangle_{iso}\}$, $\Re\{\langle P^{\alpha,\beta,\alpha,\beta}_{z,z,z,z}(\tau,T,t)\rangle_{iso}\}$, and $\Im\{\langle P^{\alpha,\beta,\alpha,\beta}_{z,z,z,z}(\tau,T,t)\rangle_{iso}\}$, which contain information about $\Re\{\chi_{\alpha\beta\alpha\beta}(T)\}$ and $\Im\{\chi_{\alpha\beta\alpha\beta}(T)\}$. By proceeding as in the previous paragraph, it can be seen that either the first two or the last two are good enough to extract information about the latter two quantities.

The steps above can repeated for the rest of the elements of $\chi(T)$ in order to select sixteen out of the thirty-two measurements which yield the desired QPT. Table S7 presents an adaptation

of Table S3, where, in the first column, we show a possible set of experiments which yields QPT for the case of $\mathcal{G}_{gp}(\tau)\mathcal{G}_{ps}(t)$ being purely real.

Table S7. A set of only sixteen measurements which yields $\chi(T)$ for the case $\mathcal{G}_{gp}(\tau)\mathcal{G}_{ps}(t) \in \Re$

From the data	we can invert the elements	which explicitly listed are
$\left\{\begin{array}{c}\Re\{\langle P^{\alpha,\alpha,\alpha,\alpha}_{z,z,z,z}(\tau,T,t)\rangle_{iso}\},\\ \Re\{\langle P^{\alpha,\alpha,\alpha,\beta}_{z,z,z,z}(\tau,T,t)\rangle_{iso}\},\\ \Im\{\langle P^{\alpha,\alpha,\alpha,\beta}_{z,z,z,z}(\tau,T,t)\rangle_{iso}\},\\ \Re\{\langle P^{\alpha,\alpha,\beta,\beta}_{z,z,z,z}(\tau,T,t)\rangle_{iso}\}\end{array}\right\}$	$\{\chi_{ij\alpha\alpha}(T)\}$	$\left\{\begin{array}{c}\chi_{\alpha\alpha\alpha\alpha}(T),\\ \chi_{\beta\beta\alpha\alpha}(T),\\ \Re\{\chi_{\alpha\beta\alpha\alpha}(T)\} = \Re\{\chi_{\beta\alpha\alpha\alpha}(T)\},\\ \Im\{\chi_{\alpha\beta\alpha\alpha}(T)\} = -\Im\{\chi_{\beta\alpha\alpha\alpha}(T)\}\end{array}\right\}$
$\left\{\begin{array}{c}\Re\{\langle P^{\beta,\beta,\alpha,\alpha}_{z,z,z,z}(\tau,T,t)\rangle_{iso}\},\\ \Re\{\langle P^{\beta,\beta,\alpha,\beta}_{z,z,z,z}(\tau,T,t)\rangle_{iso}\},\\ \Im\{\langle P^{\beta,\beta,\alpha,\beta}_{z,z,z,z}(\tau,T,t)\rangle_{iso}\},\\ \Re\{\langle P^{\beta,\beta,\beta,\beta}_{z,z,z,z}(\tau,T,t)\rangle_{iso}\}\end{array}\right\}$	$\{\chi_{ij\beta\beta}(T)\}$	$\left\{\begin{array}{c}\chi_{\alpha\alpha\beta\beta}(T),\\ \chi_{\beta\beta\beta\beta}(T),\\ \Re\{\chi_{\alpha\beta\beta\beta}(T)\} = \Re\{\chi_{\beta\alpha\beta\beta}(T)\},\\ \Im\{\chi_{\alpha\beta\beta\beta}(T)\} = -\Im\{\chi_{\beta\alpha\beta\beta}(T)\}\end{array}\right\}$
$\left\{\begin{array}{c}\Re\{\langle P^{\beta,\alpha,\alpha,\alpha}_{z,z,z,z}(\tau,T,t)\rangle_{iso}\},\\ \Im\{\langle P^{\beta,\alpha,\alpha,\alpha}_{z,z,z,z}(\tau,T,t)\rangle_{iso}\},\\ \Re\{\langle P^{\beta,\alpha,\alpha,\beta}_{z,z,z,z}(\tau,T,t)\rangle_{iso}\},\\ \Im\{\langle P^{\beta,\alpha,\alpha,\beta}_{z,z,z,z}(\tau,T,t)\rangle_{iso}\},\\ \Re\{\langle P^{\beta,\alpha,\beta,\beta}_{z,z,z,z}(\tau,T,t)\rangle_{iso}\},\\ \Im\{\langle P^{\beta,\alpha,\beta,\beta}_{z,z,z,z}(\tau,T,t)\rangle_{iso}\},\\ \Re\{\langle P^{\beta,\alpha,\beta,\alpha}_{z,z,z,z}(\tau,T,t)\rangle_{iso}\},\\ \Im\{\langle P^{\beta,\alpha,\beta,\alpha}_{z,z,z,z}(\tau,T,t)\rangle_{iso}\}\end{array}\right\}$	$\{\chi_{ij\alpha\beta}(T) = (\chi_{ji\beta\alpha}(T))^*\}$	$\left\{\begin{array}{rcl}\Re\{\chi_{\alpha\alpha\alpha\beta}(T)\} &=& \Re\{\chi_{\alpha\alpha\beta\alpha}(T)\},\\ \Im\{\chi_{\alpha\alpha\alpha\beta}(T)\} &=& -\Im\{\chi_{\alpha\alpha\beta\alpha}(T)\},\\ \Re\{\chi_{\beta\beta\alpha\beta}(T)\} &=& \Re\{\chi_{\beta\beta\beta\alpha}(T)\},\\ \Im\{\chi_{\beta\beta\alpha\beta}(T)\} &=& -\Im\{\chi_{\beta\beta\beta\alpha}(T)\},\\ \Re\{\chi_{\alpha\beta\alpha\beta}(T)\} &=& \Re\{\chi_{\beta\alpha\beta\alpha}(T)\},\\ \Im\{\chi_{\alpha\beta\alpha\beta}(T)\} &=& -\Im\{\chi_{\beta\alpha\beta\alpha}(T)\},\\ \Re\{\chi_{\beta\alpha\alpha\beta}(T)\} &=& \Re\{\chi_{\alpha\beta\beta\alpha}(T)\},\\ \Im\{\chi_{\alpha\beta\alpha\beta}(T)\} &=& -\Im\{\chi_{\beta\alpha\beta\alpha}(T)\}\end{array}\right\}$

The same calculation of Fig. S2 can be repeated for this setting, where $\mathbb{M}^{qp}$ and $P^{qp}(T)$ only contain the elements in the first column of Table S7. We do not show them because they have the same coarse appearance as the ones in Fig. S2. We make a numerical comparison between the matrices of κ values calculated in the previous subsection and the ones computed with the selective measurements of Table S7, where we round large values of κ down to be 100. We find relative differences in their 2-norms of 0.094, 0.12, 0.0023, and 0.0028 for the d_B/d_A =1, 1.5, 10, 150 cases, respectively, supporting the qualitative claim that the two protocols are similar in terms of stability.

XII. SCALABILITY

The QPT protocol can be extended to general aggregates of d chromophores using a pulse toolbox of d different waveforms (the single exciton Hilbert space is size d). Details will be provided in a future publication. For now, let us make a comparison between the number of

1D measurements required for a multichromophoric QPT and the effort involved in collecting a standard 2D-ES [26]On the one hand, without keeping track of leakage errors, the number of required QPT 1D experiments is equal to the number of parameters to extract, $d^4 - d^2$. On the other hand, the number of grid points in a single 2D-ES, which we take as the effective number of experiments, is on the order of 7000 [21]. Therefore, within this crude measure, it is only for $d > 10$ that a QPT becomes more costly than a single 2D-ES [27] . Clearly, the scalability of QPT as $O(d^4)$ is not favorable asymptotically, although ideas associated with single shot setups [22] or compressed sensing [23, 24] could provide significant reductions in the required physical resources. However, this limit might not even be relevant at present. So far, the largest multichromophoric system for which spectral lineshapes can be resolved in a 2D-ES consists of the lowest lying states of the Light Harvesting Complex-II [25], corresponding to $d = 14$, giving $14^4 - 14^2 = 38220$ 1D experiments, which amounts to an effort of collecting about six 2D-ES.

---

[1] M.D. Choi. Completely positive linear maps on complex matrices. *Linear Algebra Appl.*, 10(3):285 – 290, 1975.

[2] E. C. G. Sudarshan, P. M. Mathews, and Jayaseetha Rau. Stochastic dynamics of quantum-mechanical systems. *Phys. Rev.*, 121(3):920–924, 1961.

[3] T. Mančal and G. R. Fleming. Probing electronic coupling in excitonically coupled heterodimer complexes by two-color three-pulse photon echoes. *J. Chem. Phys.*, 121:10556–10565, 2004.

[4] J. Yuen-Zhou and A. Aspuru-Guzik. Quantum process tomography of excitonic dimers from two-dimensional electronic spectroscopy. i. general theory and application to homodimers. *J. Chem. Phys.*, 134(13):134505, 2011.

[5] S. Mukamel. *Principles of Nonlinear Optical Spectroscopy.* Oxford University Press, 1995.

[6] D.P. Craig and T. Thirunamachandran. *Molecular quantum electrodynamics: An introduction to radiation molecule interactions.* Dover Publications, 1998.

[7] A. M. Kuah, K. Modi, C. A. Rodríguez-Rosario, and E. C. G. Sudarshan. How state preparation can affect a quantum experiment: Quantum process tomography for open systems. *Phys. Rev. A*, 76(4):042113, 2007.

[8] K. Modi and E. C. G. Sudarshan. Role of preparation in quantum process tomography. *Phys. Rev. A*, 81(5):052119, 2010.

[9] K. Modi. Non-Markovian memory in quantum process tomography and a preparation independent map. *ArXiv e-prints*, 2010.

[10] H. Lee, Y. C. Cheng, and G. R. Fleming. Coherence Dynamics in Photosynthesis: Protein

Protection of Excitonic Coherence. *Science*, 316:1462–1465, 2007.

[11] Hochstrasser R. M. Two-dimensional ir-spectroscopy: polarization anisotropy effects. *Chem. Phys.*, 266(2-3):273 – 284, 2001.

[12] G. S. Schlau-Cohen, T. R. Calhoun, N. S. Ginsberg, M. Ballottari, R. Bassi, and G. R. Fleming. Spectroscopic elucidation of uncoupled transition energies in the major photosynthetic light-harvesting complex, LHCII. *Proc. Natl. Acad. Sci. USA*, 107(30):13276–13281, 2010.

[13] D.B. Strasfeld, C.T. Middleton, and M.T. Zanni. Mode selectivity with polarization shaping in the mid-ir. *New J. Phys.*, 11(10):105046, 2009.

[14] M. Cho. *Two Dimensional Optical Spectroscopy.* CRC Press, 2009.

[15] D. M. Jonas. Two-dimensional femtosecond spectroscopy. *Ann. Rev. Phys. Chem.*, 54:425–463, 2003.

[16] S. M. Gallagher Faeder and D. M. Jonas. Two-dimensional electronic correlation and relaxation spectra: Theory and model calculations. *J. Phys. Chem. A*, 103(49):10489–10505, 1999.

[17] V. May and O. Kuhn. *Charge and Energy Transfer Dynamics in Molecular Systems.* Wiley-VCH, 2004.

[18] A. V. Pisliakov, T. Mančal, and G. R. Fleming. Two-dimensional optical three-pulse photon echo spectroscopy. ii. signatures of coherent electronic motion and exciton population transfer in dimer two-dimensional spectra. *J. Chem. Phys.*, 124:234505, 2006.

[19] W. Cheney and D. Kincaid. *Numerical mathematics and computing.* Thomson-Brooks/Cole, sixth edition, 2008.

[20] R. A. Horn and Johnson C. R. *Matrix Analysis.* Cambridge University Press, 1990.

[21] M. T. Zanni, S. Gnanakaran, J. Stenger, and R. M. Hochstrasser. Heterodyned two-dimensional infrared spectroscopy of solvent-dependent conformations of acetylproline-nh2. *J. Phys. Chem. B*, 105(28):6520–6535, 2001.

[22] E. Harel, A. F. Fidler, and G. S. Engel. Real-time mapping of electronic structure with single-shot two-dimensional electronic spectroscopy. *Proc. Natl. Acad. Sci. USA*, 107(38):16444–16447, 2010.

[23] M. Mohseni, A. T. Rezakhani, and D. A. Lidar. Quantum-process tomography: Resource analysis of different strategies. *Phys. Rev. A*, 77:032322, 2008.

[24] A. Shabani, R. L. Kosut, M. Mohseni, H. Rabitz, M. A. Broome, M. P. Almeida, A. Fedrizzi, and A. G. White. Efficient measurement of quantum dynamics via compressive sensing. *Phys. Rev. Lett.*, 106(10):100401, 2011.

[25] T. R. Calhoun, N. S. Ginsberg, G. S. Schlau-Cohen, Y. C. Cheng, M. Ballottari, R. Bassi, and G. R. Fleming. Quantum coherence enabled determination of the energy landscape in light-harvesting complex ii. *J. Phys. Chem. B*, 113(51):16291–16295, 2009.

[26] Contrasting the number of experiments in two different settings does not necessarily provide a fair estimate of the real effort, as an experimentalist might have built a machine that efficiently carries one type of measurement, but not the other. However, at least this provides an estimate of the resources involved in each situation.

[27] As explained in point (b) above, QPT can also be performed with 2D-ES, but for large d values, precisely due to the reasons just outlined, the 1D setup is more convenient.